The Dual Molecular Identity of Vestibular Kinocilia: Bridging Structural and Functional Traits of Primary and Motile Cilia

Zhenhang Xu[1]†, Amirrasoul Tavakoli[2]†*, Samadhi Kulasooriya[1], Huizhan Liu[1], Shu Tu[1], Celia Bloom[1], Yi Li[1], Tirone D. Johnson[2], Jian Zuo[1], Litao Tao[1], Bechara Kachar[2*], David Z. He[1*]

[1]Department of Biomedical Sciences, Creighton University, Omaha, Nebraska 68178
[2]Laboratory of Cell Structure and Dynamics, National Institute on Deafness and Other Communication Disorders, National Institutes of Health, Bethesda, Maryland 20892

†These authors contribute equally

*Corresponding authors
Amirrasoul Tavakoli: amir.tavakolitarghi@nih.gov
Bechara Kachar: kacharb@nidcd.nih.gov
David Z. He: hed@creighton.edu

Present affiliation:
ZX: Department of Otorhinolaryngology – Head and Neck Surgery, Xiangya Hospital, Central South University, Changsha, China
YL: Department of Otorhinolaryngology – Head and Neck Surgery, Beijing Tongren Hospital, Capital Medical University, Beijing, China
ST: Harvard School of Dental Medicine, Boston, MA 02115
JZ: Ting Therapeutics, San Diego, CA 92121

ABSTRACT

Vestibular hair cells (HCs) convert gravitational and head motion cues into neural signals through mechanotransduction, mediated by the hair bundle—a mechanically integrated organelle composed of stereocilia and a kinocilium. The kinocilium, a specialized form of primary cilium, remains incompletely defined in structure, molecular composition, and function. To elucidate its characteristics, we conducted single-cell RNA sequencing of adult vestibular and cochlear HCs, uncovering a selective enrichment of primary and motile cilia–associated genes in vestibular HCs, particularly those related to the axonemal repeat complex. This enrichment of orthologous axonemal-related genes was conserved in zebrafish and human vestibular HCs, indicating a shared molecular architecture. Immunostaining validated the expression of key motile cilia markers in vestibular kinocilia. Moreover, live imaging of bullfrog and mouse HCs from crista ampullaris revealed spontaneous kinociliary motion. Together, these findings define the kinocilium as a unique organelle with molecular features of primary and motile cilia and suggest its previously unknown role as an active, force-generating element within the hair bundle.

KEY WORDS

Vestibule, cochlea, hair cell, kinocilia, motile cilia, axoneme, transcriptome, mouse, bullfrog, human

INTRODUCTION

The mammalian inner ear contains auditory and vestibular end organs, which detect sound and motion signals respectively. Hair cells (HCs), the sensory receptors found in both these structures, transduce mechanical stimuli in the form of sound or head movement into electrical signals (Fettiplace, 2017; Gillespie and Müller, 2009). The HCs of the auditory sensory epithelium in the cochlea are categorized as inner and outer HCs (IHCs and OHCs) (Dallos, 1992). The vestibular sensory epithelium lining two otolith organs (utricular and saccular maculae) and three cristae associated with semicircular canals also contains two types of HCs—type I and type II—based on morphology, physiology, and innervation (Eatock et al., 1998; Eatock and Songer, 2011).

Although mechanotransduction is a shared feature of all HCs, mammalian cochlear and vestibular HCs differ in morphology and function. One key difference lies in the structure of the hair bundle, which harbors specialized machinery for mechanotransduction. The hair bundle of adult vestibular HCs is composed of actin-rich stereocilia connected via lateral links to a single microtubule-based kinocilium, meanwhile cochlear HCs lose their kinocilia during HC maturation (Leibovici et al., 2005). Kinocilia are highly conserved in non-mammalian vertebrates (Leibovici et al., 2005) and play a pivotal role in establishing hair bundle polarity and mediating Hedgehog and WNT signaling during HC development (Moon et al., 2020; Shi et al., 2022). Despite possessing features of motile cilia such as the canonical “9+2” microtubule arrangement, the kinocilium has long been regarded as a specialized primary cilium (Kikuchi et al., 1989; Wang and Zhou, 2021). While the kinocilium contributes to the bundle mechanics (Baird, 1994; Kindt et al., 2012; Spoon and Grant, 2011), the molecular basis and function of this unique organelle in adult vestibular HCs remain unknown.

In the current study we utilized single-cell RNA-sequencing (scRNA-seq) to examine the transcriptomes of 1,522 HCs isolated from cochlear and vestibular sensory epithelia of adult CBA/J mice Comparisons of the molecular profiles of the four HC types identified novel marker genes as well as shared and unique genes associated with mechanotransduction, ion channels, and pre- and post-synaptic structures. Notably, our analysis revealed a significant enrichment of genes related to primary and motile cilia in vestibular HCs, particularly those linked to the 96-nm axonemal repeat complex, a hallmark feature of motile cilia. Orthologous axonemal-related genes were also detected in zebrafish HCs and human vestibular HCs. We utilized transmission electron microscopy (TEM) to examine the ultrastructure of kinocilia and immunostaining to detect expression of key motile cilia proteins in vestibular HCs. We also used live imaging to examine

kinocilia motion in bullfrog and mouse crista ampullaris. We modeled the atomic architecture of the 96-nm repeat, the core framework of the kinocilium axoneme. Together, these findings establish the kinocilium as a distinct organelle with molecular hallmarks of motile cilia and suggest it functions as an active, force-generating hair bundle component, influencing the mechanosensitivity of the kinocilium-bearing HCs across nonmammalian and mammalian species. In addition, our transcriptomic analysis provides new insight into the molecular mechanisms underlying phenotypical differences among the four different HC types in the adult mouse inner ear.

RESULTS

Solitary cells were isolated from the whole basilar membrane (together with the organ of Corti, Fig. 1A) and vestibular end organs from 10-week-old CBA/J mice. Cells isolated from the cochlea include IHCs, OHCs, supporting cells (SCs), spiral ganglion neurons (SGNs), and other accessory cells. Some examples of individual IHCs and OHCs are shown in Fig. 1A. Cells isolated from vestibular sensory epithelia include type I HCs, type II HCs, SCs, vestibular neurons and other cell types. Vestibular HCs can be identified based on morphological features: Type I HCs are flask-shaped with a narrow neck while type II HCs are cylindrical and short (Burns and Stone, 2017; Eatock et al., 1998; Lysakowski and Goldberg, 1997; Pujol et al., 2014; Ricci et al., 1997). Type II HCs and SCs also express *Sox2*/SOX2 (Fig. 1B), which is a marker for these cell types in the vestibular sensory epithelium (Jan et al., 2021; Wilkerson et al., 2021). Some representative images of type I and type II HCs isolated from maculae of utricle and saccule as well as from crista ampullaris are presented in Fig. 1C.

To comprehensively assess the molecular profiles of inner ear HCs, we conducted scRNA-seq using cells isolated from the auditory and vestibular sensory epithelia. The within-tissue cellular diversity and identity in the cochlear and vestibular sensory epithelia were assessed by a t-distributed Stochastic Neighbor Embedding (t-SNE) analysis followed by clustering and annotations of cell types based on the expression of known marker genes (Fig. 1D,E)(Burns et al., 2015; Jan et al., 2021; McInturff et al., 2018; Ranum et al., 2019; Wilkerson et al., 2021). Upon cluster annotation and normalization across biological repeats, HC types were separated for the downstream analysis by their known marker genes shown in feature plots (Fig. 1F) and dot plots (Fig. 1G). A total of 1,522 individual cells were identified as HCs, including 131 IHCs, 668 OHCs, 588 type I HCs, and 135 type II HCs for our downstream analysis. We aggregated the number of

reads for each gene across all single cells to generate pseudo-bulk expression profiles for different HC types (Table S1).

1. Similarities among HC types

We utilized the pseudo-bulk and single-cell gene expression profiles to compare the four HC types. Since adult IHC and OHC transcriptomes have been compared extensively in the past (Li et al., 2018; Ranum et al., 2019), we focused our analyses on the differences between cochlear and vestibular HCs, as well as between type I and type II HCs. Principal component analysis (PCA) was used to denote variance across the four types of HCs. The first principal component (PC1) shows that the most dramatic differences are tissue-based—between cochlear and vestibular HCs (Fig. 2A). The distribution across PC2 indicates that the similarity between type I and type II HCs is greater than the similarity between IHCs and OHCs, suggesting more homogeneity among vestibular HCs. Gene expression profiles of single HCs were also used to analyze similarities among the four different HC types (Fig. 2B). Despite heterogeneity found among individual HCs of each type, three-dimensional PCA visualization of single cells draws similar conclusions to the pseudo-bulk PCA, suggesting higher transcriptomic similarity between vestibular HCs in contrast to cochlear HCs.

2. Differentially expressed genes in HC types

Next, we examined the number of genes that are shared and unique among the four types of HCs based on pseudo-bulk expression profiles (Fig. 2C). Although approximately 71% of the detected genes are shared among all four types of HCs, the smaller proportion of unique genes in each HC population may underlie their specific biological identities. We performed pairwise differentially expressed gene (DEG) analyses between within-tissue HC types, as well as between cochlear and vestibular HCs (Fig. 2D). DEGs were defined as those with an expression level above 0 and a minimum of 2-fold change (log2 $\geq$ 1) between the two cell populations with statistical significance of $p \leq 0.01$.

DEGs between adult IHCs and OHCs have been analyzed before using cell type-specific microarray and bulk RNA-seq techniques (Li et al., 2018; Liu et al., 2014). Here, our comparison revealed differential enrichment of 154 and 123 genes in IHCs and OHCs respectively (Fig. 2D). We show expression of previously characterized DEGs in IHCs (e.g., *Otof*, *Slc17a8*) and OHCs (e.g., *Ocm*, *Slc26a5*, *Chrna10*) as well as genes whose functions have not yet been characterized, including *Atp2a3*, *Calb2*, *Dnajc5b*, *Ripor3*, and *Scd1* in IHCs, and *Aqp11*, *Dnm3*, and *Sh3gl3* in OHCs. Our DEG analysis comparing IHCs and OHCs is consistent with the previous studies (Li et

143 al., 2018; Liu et al., 2014).

144 We next compared DEGs between type I and type II HCs (Fig. 2D). Although some new marker
145 genes of adult type I and type II HCs from mouse utricles have been identified (McInturff et al.,
146 2018), differential gene expression analysis between type I and type II HCs has not been
147 conducted extensively. Our analysis revealed enrichment of 35 DEGs in type I HCs and 59 DEGs
148 in type II HCs. Except for a few genes such as *Otog* and *Bmp2*, the roles of these DEGs in
149 vestibular HCs have not been examined.

150 Grouping the tissue-specific subtypes together, we calculated DEGs between cochlear and
151 vestibular HCs (Fig. 2D). This comparison identified 674 DEGs enriched in cochlear HCs and 887
152 DEGs enriched in vestibular HCs. We note that many vestibular DEGs (such as *Adam11*, *Car12*,
153 *Nrxn3*, *Lpgat1*, *Spp1*, *Pcdh20*, *Cfap126*) are related to the secretion of extracellular matrix protein,
154 cell-matrix interactions, cell adhesion, mineralized matrix, calcification, acid-base balance, and
155 cilia. Meanwhile, many of the genes enriched in cochlear HCs (such as *Slc25a5*, *Strip2*, *C1ql1*,
156 *Rorb*, and *Ocm*) are related to the extensively studied unique structure and function of cochlear
157 HCs. It is interesting that *Cib2* is differentially expressed in cochlear HCs while *Cib3* is enriched
158 in vestibular HCs. *Cib2* and *Cib3* act as an auxiliary subunit of the sensory mechanoelectrical
159 transduction (MET) channel in HCs (Giese et al., 2017; Riazuddin et al., 2012; Wang et al., 2023)
160 and mutations of these two genes are associated with deafness and Usher syndrome 1J
161 (Riazuddin et al., 2012).

162 To examine the functional relevance of the calculated DEGs, we conducted
163 overrepresentation analysis (ORA). Since the molecular properties of vestibular HCs are less
164 known compared to cochlear HCs, we looked more closely at the biological processes enriched
165 in vestibular HCs compared to cochlear HCs, which included gene ontology (GO) terms related
166 to cilium organization and microtubule-based cilia motility (highlighted by red asterisks in Fig. 2E).
167 We also conducted ORA between type I and type II HCs. In type I HCs, enriched processes
168 included those related to cytoplasmic translation, p53-mediated signal transduction, actin filament
169 depolymerization and regulation, and cilium or flagellum-dependent cell motility (Fig. 2F). Terms
170 enriched in type II HCs are related to oxidative phosphorylation, proton transmembrane transport,
171 aerobic and cellular respiration, detection of mechanical stimulus involved in sound perception
172 and mechanoreceptor differentiation (Fig. 2G).

173 **3. Marker genes for different HC types and genes related to HC specialization**

174 Previous studies have characterized some marker genes in different HC types. We assessed

175 the expression of previously characterized and newly identified genes related to HC structure and
176 function across all four HC types. Many genes are expressed in all four HC types (Fig. 3A). Among
177 these are well-characterized genes such as *Cib2*, *Otof*, *Kcna10*, *Ptprq*, *Tmc1*, and *Espn*, while
178 other genes such as *Tjap1*, which encodes a tight junction-associated protein, are less known. We
179 noted genes that were enriched in a tissue-specific manner. For example, *Cdh23*, *Rorb* and *Osbp2*
180 are more highly expressed in cochlear HCs than in vestibular HCs, while genes such as *Ldhb*,
181 *Fbxo32*, *and Gsn* are enriched in vestibular HCs but only weakly expressed in cochlear HCs.
182 Several genes expressed in vestibular HCs with no expression in cochlear HCs (such as *Cfap43*,
183 *Cfap126*, *Cib3*, *Cxcl14*, *Pcdh20*, *Pifo*, *Slc9a3r2*, *Tmc2*) could potentially be used as vestibular HC
184 markers (Fig. 3A). Moreover, *Adam11*, *Cacna2d4*, *Car12*, and *Shank2* are found to be only
185 expressed in type I HCs, while *Ccer2*, *Cfap45*, *Dlk2*, and *Rprm* are only expressed in type II HCs.
186 Our analysis also revealed new marker genes for IHCs (*Atp2a3*, *Rims2*, *Ripor3*) and OHCs (*Aqp11*,
187 *Mmd*, *Sh3gl3*). *Cfap43*, *Cfap44*, *Cfap45*, *Cfap126*, *Kif3*, *Mlf1* and *Pifo*, enriched in vestibular HCs,
188 are all associated with kinocilium structure and function. We utilized single-molecule fluorescent
189 *in situ* hybridization (smFISH) and immunostaining techniques to validate the expression of 12
190 genes in HCs (Fig. 3B, C). The expression patterns of these genes and proteins were highly
191 consistent with our observations from scRNA-seq analysis. Overall, our results identified novel
192 marker genes and previously unidentified expression patterns among the four HC types.

193 Next, we focused our analysis on evaluating the genes associated with HC function. We
194 compared the expression of 208 genes related to HC structure and function, including stereocilia
195 and apparatus for mechanotransduction, ion channels, and synapses (Fig. 4A). Among the genes
196 associated with stereocilia and mechanotransduction apparatus (Shin et al., 2013), *Calm1*, *Calm2*,
197 *Eps8*, *Espn*, *Fbxo2*, *Dynll2*, *Ush1c*, *Ywhae*, *Tmc1*, *Tmie*, *Cdh23*, *Pcdh15*, *Ank1*, *Ank3*, and *Lhfpl5*
198 were highly expressed in all four HC populations. Others were highly expressed in only one or
199 two HC populations. *Atp2a3*, *Calb2*, and *Dpysl2* were highly expressed in IHCs, while *Lmo7*, *Ocm*,
200 and *Strc* were highly expressed in OHCs. Moreover, expression of *Dpysl2*, *Cdh23*, and *Cib2* was
201 higher in cochlear HCs than in vestibular HCs, while *Xirp2*, *Pls1*, *Slc9a3r2*, and *Tubb4b* were more
202 highly expressed in vestibular HCs than in cochlear HCs. Some genes were uniquely expressed
203 in either cochlear or vestibular HCs. For example, *Cib3* and *Tmc2* are expressed in vestibular HCs
204 but not in cochlear HCs.

205 All HCs possess ion channels. Our analysis detected several genes related to stretch-activated
206 ion channels, such as *Trpc1* and *Trpm4.* Genes for Cl^- and Na^+ channels were expressed. For Ca^{2+}

and K^+ channels, *Cacna1d and Kcna10* were expressed in all four HC types with varying levels of expression. In cochlear HCs, *Cacna1d, Kcna10, Kcnab1, Kcnj16 and Kcnma1* were expressed in IHCs, whereas *Cacna1d, Kcna10, Kcnk1, Kcnma1, Kcnn2* and *Kcnq4* were expressed in OHCs. In the vestibular HCs, *Cacna2d4, Kcna10, Kcnab1,* and *Kcnma1* showed relatively high expression in type I HCs whereas type II HCs indicated a relatively high expression of *Cacna2d4, Cacng5, Kcna10, Kcnb1, Kcnh2,* and *Kcnh7*. *Best1, Clic, Hcn1,* and *Kcnh7* were only expressed in vestibular HCs.

Next, we examined the genes related to synapses (Fig. 4A). Our results indicated expression of *Ctpb2*, *Dlg1*, *Homer2*, *Otof*, *Pclo*, and *Snap91* in all HCs at varying levels. We observed a relative higher expression of *Dnm1*, *Otof*, *Rims2*, *Slc17a8*, *Snap91*, and *Stx7* in IHCs while *Dlg1*, *Dnm3*, *Snap9*, *Chrna9*, and *Chrna10* showed higher expression in OHCs. Some of the highly expressed genes in type I HCs include *Dnm1*, *Kif3a*, *Pclo*, *Shank2*, *Slc17a8*, *Syt13*, *Syt14*, *Chrna9*, and *Chrna10*, whereas type II HCs showed relatively higher expression of *Kif3a*, *Otof*, *Shank2*, *Stx7*, and *Syt13*. We employed smFISH to validate the expression of 8 additional genes across the four HC types. The expression patterns shown in Fig. 4B are consistent with our analysis (Fig. 4A).

4. Gene signatures of primary cilia in cochlear and vestibular HCs

A key morphological feature in the hair bundle of vestibular HCs is the presence of kinocilium, which has been regarded as a type of specialized primary cilia. Since our analysis revealed an enrichment of cilium-related GO terms (Fig. 2F) and axonemal genes such as *Cfap43, Cfap44, Cfap45, Cfap126, Kif3, Plf1,* and *Tubb4b* (Fig. 3A) in vestibular HCs, we sought to investigate the composition and molecular nature of the kinocilium (Fig. 5A). Proteomics-based approaches have contributed to the development of cilia-associated protein databases. We utilized several well-established databases, including CiliaCarta (Dam et al., 2019), the SYSCILIA gold standard (SCGSv2)(Vasquez et al., 2021), and CilioGenics (Pir et al., 2024) to compile a list of ~1,000 cilia-related genes. We noted a significant overlap of these genes with our HC transcriptomic profiles (Fig. 5B). GO analysis of the overlapping genes revealed enrichment of cellular component and biological process terms primarily related to cilia organization, assembly, maintenance, intracellular transport, and microtubule dynamics particularly associated with motile cilia (Fig. S1). Additionally, molecular function analysis highlights associations with motor activity, dynein chain binding, and BBSome binding (Fig. S1). BBSome (Bardet-Biedl syndrome) is an octameric protein complex crucial for regulating transport in primary cilia (Tian et al., 2023).

The primary cilium is a sensory organelle that responds to and transmits external signals to

239 the cell's interior. Structurally, primary cilia are characterized by the presence of nine microtubule
240 doublets (MTDs) encircling the shaft, which transition into a disorganized structure distally (Fig.
241 5C). We first examined the expression of primary cilia-related genes in vestibular and cochlear
242 HCs. Among approximately 420 primary cilia-related genes/proteins (Dam et al., 2019; Pir et al.,
243 2024; Vasquez et al., 2021), we detected the expression of 410 genes in at least one type of HC.
244 Fig. 5D shows the top 50 abundantly expressed primary cilia-related genes in type II HCs
245 compared to the other three HC types. Most of these genes were detected in all four HC types
246 except a few genes, such as *Mlf1, Ttc21a,* and *Tmem218,* which were weakly or not expressed in
247 cochlear HCs.

248 Primary cilia are enriched in receptors and effectors for key pathways, including GPCR, cAMP,
249 Ca^{2+}, RTK, TGF-β, MAPK, TOR, BMP, Wnt, Notch, and Rho signaling (Anvarian et al., 2019),
250 localized to the ciliary shaft, transition zone, and BBSome (Hansen et al., 2025). We analyzed the
251 expression of these genes in HCs and found higher expression levels of these pathway-related
252 genes in vestibular HCs than in cochlear HCs (Fig. S2).

253 Intraflagellar transport (IFT) involves anterograde and retrograde transport of molecules along
254 the axoneme of cilia, facilitating the transport of components between the ciliary base and tip
255 (Ma et al., 2023). IFT is essential for the proper assembly and maintenance of both primary and
256 motile cilia. Thus, we assessed the expression of IFT-associated genes in HCs. Most of the
257 genes are enriched in vestibular HCs compared to cochlear HCs (Fig. 5D). Immunostaining
258 confirmed the expression of IFT172 and CLUAP1 in the kinocilia of vestibular HCs (Fig. 5E).

259 **5. Gene signatures of motile cilia in vestibular HCs**

260 Curiously, our GO analysis returned many terms related to cilium motility. Motile cilia are highly
261 conserved organelles across different organisms and tissues, although they exhibit organism- and
262 tissue-specific adaptations (Leung et al., 2025). Recent advances using proteomics of isolated
263 motile cilia from various ciliated tissues have enabled the profiling of genes associated with motile
264 cilia. To explore whether the kinocilium possesses a molecular composition characteristic of
265 motile cilia, we compared our HC transcriptomes with multi-tissue proteomics datasets derived
266 from different organisms, including human, bovine, porcine, and murine, as well as diverse motile
267 ciliary tissues such as sperm, oviduct, ventricle, and trachea (Leung et al., 2025) (Fig. S3). Our
268 analysis revealed a significant overlap, particularly among axonemal components of motile cilia,
269 with strong enrichment in vestibular HCs compared to cochlear HCs. The axoneme of motile cilia
270 and flagella is a cylindrical structure harboring a canonical “9+2” arrangement, where nine doublet

271 microtubules (DMTs) surround two microtubule singlets in the center (Fig. 5C). Altogether, the
272 axoneme machinery consists of nine DMTs, two rows of inner and outer dynein arms (IDAs and
273 ODAs), nexin-dynein regulatory complex (N-DRC), two singlet central pair complex (CPC), three
274 radial spokes (RSs), microtubule inner proteins (MIPs), and external coiled-coil regions. The
275 motility unit is arranged in a 96-nm repeat module along the CPC. Recent cryo-EM and cryo-
276 electron tomography (cryo-ET) studies have provided a more comprehensive identification of this
277 module repeat (Chen et al., 2023; Leung et al., 2025; Walton et al., 2023). To understand the
278 molecular composition and function of kinocilia, we focused our analysis on the expression of
279 genes associated with the structure of motile cilia. First, we assessed the expression of gene sets
280 related to the motile cilium and each of its structural components. We noted a robust expression
281 of motile cilia-related gene signatures in vestibular HCs, while cochlear HCs expressed little to
282 none (Fig. 5F). Next, we further assessed the expression of the key genes related to motile cilia
283 machinery (Fig. 5G), including the 96-nm module and CPC, based on the current known
284 localization from biochemistry and proteomics.

285 We examined genes related to the 96-nm axonemal repeat of mammalian epithelial cilia. This
286 structural unit contains proteins encoded by 128 genes (Gui et al., 2021). We found that 112 of
287 these genes were expressed in adult vestibular HCs (Table S2). Genes encoding axonemal dynein
288 (IDAs and ODAs), such as *Dnah5* and *Dnah6*, as well as RS components (*Wdr66, Cfap206,*
289 *Cfap61, Iqub*), N-DRC components (*Drc1, Iqca*), and MIPs (*Cfap126, Wdr63*) were predominantly
290 expressed in vestibular HCs with little to no expression in cochlear HCs (Fig. 5G). Axonemal
291 CCDC39 and CCDC40, which form external coiled-coil regions, are the molecular rulers that
292 organize the axonemal structure in the 96-nm repeating interactome and are required for the
293 assembly of IDAs and N-DRC for ciliary motility (Becker-Heck et al., 2011; Brody et al., 2025;
294 Merveille et al., 2011; Oda et al., 2014). Our results indicate a high expression of *Ccdc39* and
295 *Ccdc40* in vestibular HCs, whereas little to no expression was observed in cochlear HCs. We
296 should point out that unlike axonemal dynein proteins, which are uniquely required for cilia motility,
297 the encoded proteins of several genes in Fig. 5G (marked by red asterisks) are also expressed in
298 cytoplasm and/or are multifunctional.

299 Next, we examined expression of genes encoding transcription factors that are known key
300 regulators of ciliome gene activation, including RFX and FOXJ1 transcription factor families. RFX
301 controls genes in both motile and non-motile cilia, while FOXJ1 specifically governs motile cilia
302 formation (Choksi et al., 2014). Our data show moderate expression of *Foxj1* in vestibular HCs

303 and weak expression in cochlear HCs (Fig. 5G). Other genes that regulate motile cilia formation,
304 including *Lrrc6*, were also expressed at high to moderate levels in vestibular HCs compared to
305 cochlear HCs. We also found a strong enrichment of transcriptional targets associated with
306 vestibular HCs, particularly those involved in motile cilia programming and maintenance. The
307 expression of these transcription factors may reflect their importance in the maintenance of
308 kinocilia in adult vestibular HCs. Furthermore, analysis of a published ATAC-seq dataset (Jen et
309 al., 2019) from adult mouse vestibular tissue revealed increased chromatin accessibility in the
310 promoter regions of genes associated with motile cilia machinery (Fig. S4), suggesting elevated
311 transcriptional activity in vestibular HCs. These findings are consistent with our observations from
312 scRNA-seq datasets.

313 To examine conservation of expression of these genes in vestibular HCs across species, we
314 obtained the orthologs of axoneme-related genes in adult zebrafish inner ear HCs and human
315 vestibular HCs using published datasets (Barta et al., 2018; Wang et al., 2024). Fig. 6A shows the
316 expression of these genes in adult mouse, zebrafish, and human vestibular HCs. While the
317 expression level varies, most of these genes are expressed across species. The exceptions are
318 *Dnah3* and *Dnah12*, which are expressed in zebrafish HCs but not in mammalian vestibular HCs.

319 We conducted immunostaining and high-resolution confocal imaging to validate the
320 expression of key motile cilia markers in the kinocilia. FOXJ1 is expressed in the nucleus of
321 vestibular HCs, while CCDC39, CCDC40, TEKT1, DNAH5, and DNAH6 are expressed in kinocilia
322 (Fig. 6B). Collectively, our findings provide evidence corroborating the presence of motile cilium
323 machinery in the kinocilia of vestibular HCs.

324 Since nascent cochlear HCs possess kinocilia (Fig. 6C), we used published P2 cochlear and
325 vestibular HC transcriptomes (Burns et al., 2015; McInturff et al., 2018) to investigate whether
326 neonatal cochlear HCs express motile cilium-related genes. Assessment of expression of genes
327 related to motile cilia machinery revealed a less drastic difference between neonatal cochlear and
328 vestibular HCs than that between adult cochlear and vestibular HCs (Fig. 6D). We note that
329 proteins of some shared genes are expressed in both cilia and cytosol (marked by red asterisks
330 in Fig. 6D). However, some key motility-associated genes such as *Dnah6* and *Dnah5* (marked by
331 red arrows in Fig. 6D) were not detected in the P2 cochlear HCs. These axonemal dynein heavy
332 chains are ATPase-driven force-generating motors that produce the ciliary power stroke in
333 concert with other axonemal components. Immunostaining confirmed the lack of expression of
334 CCDC39, CCDC40, and DNAH6 in cochlear HCs at P2 (Fig. 6E). In contrast, these key proteins

335 were expressed in kinocilia of vestibular HCs (Fig. 6E). Lack of expression of *Dnah5* and *Dnah6*
336 and the molecular rulers CCDC39 and CCDC40 suggests that the kinocilium of neonatal cochlear
337 HCs does not possess signatures of motile cilia. Therefore, our analysis indicates that the
338 molecular composition of kinocilia is different between neonatal cochlear and vestibular HCs.

339 **6. Vestibular kinocilia exhibit hybrid morphological features of primary and motile cilia**

340 TEM studies have characterized the ultrastructure of kinocilia across species, revealing
341 evidence of complex and regionally specialized organization (Kikuchi et al., 1989; Nagel et al.,
342 2014; O'Donnell and Zheng, 2022). We used TEM to examine the ultrastructure of kinocilia from
343 bullfrog crista HCs. TEM images, including longitudinal sections of frog vestibular hair bundles
344 (Fig. 7A) highlight a distinct zonal architecture along the kinocilium axis. At the distal tip, a
345 prominent kinociliary bulb is observed, while the base anchors the axoneme within the cuticular
346 plate. Two pairs of microtubule doublets span the full length of the kinocilium in the longitudinal
347 section. The central pair of singlet microtubules, typical of motile cilia, is maintained throughout
348 most of the shaft but disappears in the distal and transitional zones. This configuration results in a
349 dynamic shift from a canonical 9+2 arrangement centrally to a 9+0 pattern at both the base and
350 tip. These observations underscore the heterogeneous and hybrid nature of vestibular kinocilia,
351 integrating structural features of both primary and motile cilia.

352 **7. Evidence that vestibular kinocilia exhibit motility**

353 Vestibular kinocilia are traditionally regarded as non-motile, lacking the rhythmic beating
354 characteristic of respiratory cilia. Kinocilia are not only tightly connected to stereocilia but are also
355 embedded in the overlaying gelatinous membrane (Eatock and Songer, 2011; Leibovici et al.,
356 2005; Li et al., 2008), an extracellular matrix required for physiological mechanotransduction.
357 Using acute preparations of bullfrog semicircular canal sensory epithelia (cristae), we observed
358 robust spontaneous kinociliary motility in some HCs (Fig. 7B; Videos S1 and S2). This motility
359 exhibited the characteristic beating pattern of flagella and cilia and occurred at a frequency of
360 approximately 5 - 10 Hz at room temperature. The observed displacements were sufficiently large
361 to induce deflection of the entire hair bundle, indicating it can generate forces to influence hair
362 bundle dynamics. Interestingly, this phenomenon was detected in only ~1 - 5% of crista HCs, likely
363 due to variable preservation of HC and kinociliary integrity *in vitro* in acutely dissected tissue.
364 These findings suggest that vestibular kinocilia are capable of active movement and challenge the
365 strict classification of these structures as non-motile even though motility is not experimentally
366 observed in most HCs in the excised vestibular sensory epithelium.

367 Next, we explored whether the kinocilia of vestibular HCs from adult mice are motile by utilizing
368 the photodiode technique to detect bundle motion (Jia and He, 2005). This technique can detect
369 motion in the 10-nm range for synchronized signals after averaging. Since spontaneous motions
370 are not synchronized and cannot be averaged to improve signal-to-noise ratio, we captured the
371 responses in the time domain and averaged them in the frequency domain after a fast Fourier
372 transform. This allows us to detect unsynchronized cilia motion even if the signal is close to the
373 noise level at the time domain. We first measured spontaneous cilia movement from the epithelial
374 lining of the Eustachian tube, which is an extension of airway epithelia, as cilia in the respiratory
375 tract are a typical example of motile cilia. Fig. 7C shows two representative waveforms of airway
376 cilia beat with a magnitude between 700 and 1500 nm. The two responses shown in Fig. 7C have
377 main frequency components at 6 to 9 Hz at room temperature. Next, we measured the movement
378 of the top segment of the hair bundle from mouse crista ampullaris. Since the kinocilium is tightly
379 attached to the stereocilia bundle, we measured the whole bundle's motion due to the difficulty of
380 taking measurements from a single kinocilium. The waveform (black trace in Fig. 7D) was obtained
381 from crista HCs bathed in perilymph-like solution (L-15 medium) with 2 mM of Ca^{2+}. Like the beat
382 frequency of airway cilia, kinocilia also moved at the frequency of ~7 Hz (Fig. 7D). To rule out the
383 possibility that the bundle motion is driven by the mechanotransduction-related activity (Benser
384 et al., 1996; Martin et al., 2003), we treated the crista ampullaris in Ca^{2+}-free medium with EGTA
385 for 2 minutes to break the tip-link (Assad et al., 1991; Jia et al., 2007; Kachar et al., 2000; Ricci et
386 al., 2003). Spontaneous motion was still detected (two red traces in Fig. 7D), suggesting that the
387 motion is independent of the transduction channel activity. We measured spontaneous bundle
388 motions from 52 crista HCs from six mice. Spontaneous motion was only detected in eight HCs.
389 An example of a lack of response is shown in Fig. 7D (blue trace). Although we were unable to
390 determine which of the HC subtypes were exhibiting kinocilia motility, it is conceivable that both
391 type I and type II HCs have this capability since they both express the genes related to motile cilia.
392 We note the kinocilia motion of mouse crista HCs was substantially smaller than that of airway cilia
393 (Fig. 7D) and bullfrog crista HCs.

394 **8. Predicted model of the 96-nm modular repeat in adult vestibular kinocilia**

395 Since kinocilia motility in mouse vestibular HCs is substantially smaller than the motility of
396 airway cilia, we investigated the structural basis underlying comparatively reduced motility of
397 kinocilia. This diminished motility may result from differences in the molecular composition and
398 organization of the axonemal machinery, particularly the 96-nm modular repeat that houses key

399 dynein motors and regulatory complexes. Recent advances in structure prediction powered by
400 artificial intelligence and cryo-electron microscopy (cryo-EM) have facilitated the generation of
401 highly conserved atomic models of the 96-nm axonemal repeat from human respiratory cilia and
402 bovine sperm flagella (Chen et al., 2023; Leung et al., 2025; Walton et al., 2023). We applied our
403 axonemal gene dataset to these atomic models to predict the molecular architecture of the 96-
404 nm repeat in vestibular kinocilia. By mapping the expression of known axonemal components onto
405 the structural frameworks derived from human respiratory (PDB: 8J07) (Walton et al., 2023) and
406 bovine sperm (PDB: 9FQR)(Leung et al., 2025) axonemes, we generated two composite models
407 that reflect the unique molecular composition of the vestibular kinocilium. These predicted
408 structures are shown in Figs. 8A and 8B. 3D videos of the predicted models are provided in Video
409 S3 and Video S4.

410 We chose the human respiratory 96-nm axonemal structure as our reference because it best
411 reflects vestibular kinocilia and provides a more comprehensive representation of axonemal
412 components than the sperm model, which shows more missing elements (highlighted in gold in
413 Figs. 8A,B). Using a curated reference gene list derived from the human respiratory 96-nm
414 axonemal structure, we mapped vestibular HC gene expression and identified transcripts for all
415 18 ODA genes and their docking complex components, all 11 N-DRC genes, and all 7 MAPs,
416 along with 36 of 37 RS genes and 19 of 23 IDA-related genes. Additionally, 20 of the 31 genes
417 encoding MIPs, which are known to stabilize the microtubule doublets, were also expressed (Fig.
418 5G). In contrast, vestibular HCs lacked the expression of several sperm-specific genes from
419 distinct compartments of 96-nm repeat (Leung et al., 2025), including TRiC chaperonin subunits
420 (Brown et al., 2025; X. Meng et al., 2024), CAMK4, EFACB5, LRRD1, STKLD1, CCDC63, WDR64,
421 and several MIPs (Fig. S5).

422 Based on our models, the absence of *Dnah3* and *Dnah12*, along with *Acta2*, is predicted to
423 result in the loss of two of the six single-headed IDA components (highlighted in gold). *Cfap100*,
424 which forms the modifier of inner arms (MIA) complex with *Cfap73* and contributes to tethering
425 the double-headed IDAf (inner dynein arm f), is missing in the model, whereas *Cfap73* and the
426 remaining IDAf components are present. Notably, IDAf has multiple attachment points, and MIA is
427 not essential for docking IDAf to the DMTs (Yamamoto et al., 2013). Overall, 4 of the 23 IDA-
428 related genes were not expressed in vestibular HCs; nonetheless, we predict that the IDA
429 structure is reduced but not entirely absent, as DNAH6 remains localized in vestibular kinocilia
430 (Fig. 5B). In addition to the missing IDA components, we identified 11 unexpressed genes

431 associated with MIPs, whose absence is predicted to result in reduced MIP density in the models
432 (highlighted in orchid and gold in cross-sectional views in Figs. 8A, and B). Unlike other axonemal
433 structures, MIPs exhibit greater variability across species, which may account for their lineage-
434 specific absence in vestibular kinocilia (Fig. 8)(Andersen et al., 2024; Tai et al., 2023; Xia et al.,
435 2025). The missing genes in our HC datasets and their roles in the axonemal complex, cilia motility
436 and ciliopathy are listed in Figs. 8C and S5. Based on our predicted models, we speculate that
437 the absence of *Dnah3* and *Dnah12* plays a major role in limiting kinocilia motility in mouse
438 vestibular HCs, contributing to the smaller movements compared to motile cilia.
439

440 **DISCUSSION**

441 This is the first study to compare transcriptomes among four types of HCs from the adult
442 mouse inner ear and to characterize the molecular composition of kinocilia. We found that the
443 transcriptomic similarity between type I and type II HCs is greater than that between IHCs and
444 OHCs, indicating greater homogeneity among vestibular HC subtypes compared to cochlear HC
445 subtypes. We identified several new genes and proteins that can be used as markers for vestibular
446 HCs, especially those related to kinocilia. We observed notable differences in gene signatures
447 related to HC unique structure and function, which may underlie distinct biological properties of
448 mechanotransduction, membrane conductance, and synaptic transmission seen among the four
449 different HC types. Differential expressions also explain why loss of function of a gene such as
450 *Tmc1*, *Cib2*, or *Cib3* leads to differential auditory and vestibular phenotypes in mouse models and
451 humans. Our dataset is expected to serve not only as a valuable resource for unraveling the
452 molecular mechanisms of the biological properties of HCs but also for assisting the auditory and
453 vestibular research community in identifying and exploring the functions of disease-related genes.
454 Since biological processes enriched in vestibular HCs are related to cilia and cilia motility, we
455 focused our analyses on kinocilia. Although the kinocilium has long been considered a primary
456 cilium, its molecular composition and structural organization remain largely unexplored. Our study
457 suggests that kinocilia serve dual roles as both primary and motile cilia. The primary cilium is a
458 major hub in receiving and transmitting signals from the environment. A recent study has
459 demonstrated the expression of proteins related to transduction pathways and receptors in
460 primary cilia using spatial proteomics (Hansen et al., 2024). In line with this, we found that both
461 vestibular and cochlear HCs express genes encoding components of signal transduction
462 pathways and receptors. While the precise localization of these proteins within HC kinocilia

463 remains to be validated, our analysis reveals a shared expression of diverse primary cilium
464 signaling genes across HC subtypes. This suggests a conserved, and potentially specialized, role
465 for kinocilia in cellular signaling and ciliary function.

466 Although adult cochlear HCs lack kinocilia, we still observed expression of numerous cilia-
467 related genes in in these cells (Figs. 5 and 6). While some of these genes may be vestigial, many
468 are associated with primary cilia structures, including the basal body and IFT machinery. Notably,
469 the basal body persists in adult cochlear HCs despite the developmental disappearance of the
470 kinocilium. Previous studies using cilia proteomics have shown that many cilia-related proteins
471 are expressed in cytosol, including proteins related to signal transduction, microtubule
472 cytoskeleton, actin cytoskeleton, vesicle transport, metabolism, protein folding, translation,
473 nuclear transport, ubiquitination, RNA binding, mitochondria, and transcriptional regulation (Dam
474 et al., 2019; Pir et al., 2024). Therefore, it is not unexpected that adult cochlear HCs continue to
475 express genes associated with ciliary functions.

476 A TEM study of mouse vestibular kinocilia (O'Donnell and Zheng, 2022) showed the '9+2'
477 microtubule arrangement characteristic of motile cilia. This contrasts with an earlier study of
478 guinea pig vestibular kinocilia, which reported the absence of central singlet microtubules and
479 IDAs, while ODAs and RSs were present (Kikuchi et al., 1989). In our study, TEM revealed a
480 complex and regionally specialized organization of the kinocilium in bullfrog vestibular HCs. The
481 axoneme is anchored within the cuticular plate at the kinocilium base. While the central pair of
482 singlet microtubules is preserved along most of the shaft, it is absent in the distal and transitional
483 zones—indicating a transition from the canonical 9+2 microtubule arrangement to a 9+0
484 configuration at both the base and tip. In most motile cilia, the central pair does not originate
485 directly from the basal body; instead, it begins a short distance above the transition zone, a feature
486 that illustrates variation across systems (Lechtreck et al., 2013). The central pair can also show
487 variation in its spatial extent: for example, in mammalian sperm axonemes, it can terminate before
488 reaching the distal end of the axoneme (Fawcett and Ito, 1965). In addition, the central pair
489 orientation differs across organisms: in metazoans and *Trypanosoma,* the central pair is fixed
490 relative to the outer doublets, whereas in *Chlamydomonas* and ciliates it twists within the axoneme
491 (Lechtreck et al., 2013). Such structural variation has been observed in various motile cilia and
492 flagella and is therefore not unique to vestibular kinocilia. However, a more distinctive feature of
493 kinocilium morphology is the organization at the distal tip, where a prominent distal head is
494 present—resembling tip structures recently identified in human islet cell cilia (Polino et al., 2023).

495 This distal-most region is known to harbor specialized proteins (Legal et al., 2023). In multi-ciliated
496 cells, CCDC33 and CCDC78 are found at the very end of the cilium and help organize other
497 proteins like SPEF1, CEP104, and EB3/MAPRE3 (Hong et al., 2025; Legal et al., 2024, 2023). We
498 observed expression of all genes encoding these proteins, except for *Ccdc78*. Although we did
499 not study the tip of the kinocilium, its bulb shape suggests it may also contain specialized proteins.
500 In bullfrog HCs, the kinocilial bulb binds to the overlaying otoconial membrane (Jaeger et al., 1994;
501 Kachar et al., 1990), and shows strong labeling for β-tubulin and cadherin 23 (Jaeger et al., 1994;
502 Kachar et al., 1990; Lagziel et al., 2005), and a recent study showed that *saxo2* overexpression in
503 zebrafish results in bulbed kinocilia, with *saxo2* protein accumulation at the distal tip (Erickson et
504 al., 2023). These bulbed tips may reflect specialized regulation of ciliary cap proteins (Legal et al.,
505 2023) that help organize or stabilize the plus ends of axonemal microtubules—an area that
506 remains to be explored in kinocilia.

507 The most important and novel finding of our study is that adult mouse vestibular HCs express
508 genes related to the 96-nm axonemal repeat complex, a hallmark structural feature of motile cilia.
509 Notably, orthologs of these genes are also expressed in zebrafish and human vestibular HCs,
510 highlighting the evolutionary conservation of this molecular complex across vertebrate species.
511 Furthermore, we observed robust spontaneous kinociliary motility in bullfrog crista HCs, as well
512 as subtle spontaneous bundle movements in mouse crista HCs. Our findings indicate that this
513 motion is independent of the mechanotransduction apparatus, as the kinocilium itself exhibited
514 active, flagellar-like movement in bullfrog crista HCs (Video S1 and Video S2). In mouse crista
515 HCs, spontaneous motion was still present after breaking the tip links. Early studies reported
516 observation of spontaneous flagella-like rhythmic beating of kinocilia in vestibular HCs in frogs
517 and eels (Flock et al., 1977; Rüsch and Thurm, 1990), as well as in zebrafish HCs in the early otic
518 vesicle (Stooke-Vaughan et al., 2012; Wu et al., 2011). According to Rüsch and Thurm,
519 spontaneous kinociliary motility was observed only under conditions of tissue deterioration. They
520 therefore interpreted kinocilia beating as a sign of cellular decline rather than a physiological
521 feature. We speculate that such deterioration may have disrupted kinocilial links, effectively
522 unloading the kinocilium and permitting freer movement. Nonetheless, the observation of
523 spontaneous kinocilia beating—regardless of tissue condition—supports the conclusion that they
524 are motile cilia.

525 We observed kinociliary beating in only a subset of the cells. While we cannot exclude the
526 possibility that indeed only some kinocilia are inherently motile, or that stressful conditions may

527 activate a latent motility in vestibular HCs, there are several possible reasons why such motility
528 has not been consistently observed in most vestibular HCs – both in our study and in previous
529 investigations. For example, a reduction in intracellular ATP levels in *in vitro* preparations may
530 play a significant role, as ciliary motility is ATP-dependent. Rapid depolarization of HCs *in vitro* is
531 an indication of reduced availability of intracellular ATP, as Na^+/K^+-ATPase pump is critical for
532 maintaining resting membrane potential (He and Dallos, 1999; Silver and Erecińska, 1997).
533 Additionally, acute tissue dissection may disrupt kinocilia, which are normally straight and tethered
534 to the extracellular matrix. *In vitro*, many appeared bent, potentially compromising their structural
535 integrity and the metabolic conditions required for motility.

536 Although we observed kinocilium-driven bundle movement in adult mouse vestibular HCs, its
537 magnitude was at least an order of magnitude lower than that of other motile cilia. Our single-cell
538 transcriptomic analysis showed the absence of 16 genes associated with the 96-nm axonemal
539 repeat of human respiratory cilia, including *Pierce1* and *Pierce2*. These two MIPs-encoding genes
540 have been shown to regulate motile cilia function and left–right asymmetry in mouse models (Gui
541 et al., 2021; Sung et al., 2016). *Pierce1* knockout results in pronounced defects in ciliary motility
542 and dynein arm docking, while *Pierce2* loss has a milder effect and largely preserves overall ciliary
543 ultrastructure and beating (Gui et al., 2021; Sung et al., 2016). Although the contribution of these
544 genes to kinociliary function remains uncertain, the absence of both may contribute to reduced
545 microtubule stability or motor organization, especially when combined with additional losses in
546 key motor components. However, MIPs are the most heterogeneous components across different
547 types of cilia, such as sperm and airway cilia in different species (Leung et al., 2025; Tai et al.,
548 2023). Thus, it remains unclear whether the absence of these two genes reduces kinociliary
549 motility in mouse vestibular HCs.

550 The lack of expression of two genes associated with IDAs (*Dnah12*, *Dnah3*) may lead to the
551 loss of specific single-headed IDA components as suggested by our structural models (Fig. 8).
552 Mutations of *DNAH3* and *DNAH12* are linked to male infertility and dynein dysfunction in humans
553 (Meng et al., 2024; Yang et al., 2024). Mutations of DNAH12 cause male infertility by impairing
554 DNAH1 and DNALI1 recruitment. However, it does not affect the tracheal tract and oviductal cilia
555 organization (Yang et al., 2024). For the other two IDA-related genes (*Acta2, Cfap100*/*Ccdc37*)
556 and one RS-related gene (*Morn3*), no ciliopathy has been linked to mutations of these three genes
557 so far. We speculate that the lack of expression of DNAH3 and DNAH12 may be a key factor
558 limiting magnitude of kinocilia motility in mammalian vestibular HCs compared to respiratory cilia

559 or kinocilia of bullfrog vestibular HCs.

560 We detected the expression of a few sperm-specific MIPs including *SAXO4*, *Tektin 3*, and
561 *Tektin 4* in vestibular HCs. While the kinocilium shares a broader molecular profile with epithelial
562 motile cilia, the presence of these distinct sperm-specific MIPs, which are absent from multi-
563 ciliated epithelial tissues, suggests kinocilia may possess unique structural specializations adapted
564 to their exceptional length (~60 – 70 μm in length in mouse crista HCs) and sensory function,
565 highlighting unique identity of kinocilia.

566 HCs employ positive local feedback to amplify inputs to their mechanosensitive hair bundles.
567 This amplification helps overcome mechanical impedances and fine-tune sensory stimuli. In
568 mammals, the remarkable sensitivity of the auditory system is largely attributed to the fast somatic
569 motility of OHCs in the cochlea (Brownell et al., 1985; Dallos et al., 2008; Kachar et al., 1986;
570 Liberman et al., 2002; Zheng et al., 2000). In other receptor organs, HCs may effect amplification
571 by the Ca^{2+}-dependent activity of myosin or transduction channels in the stereocilia (Fettiplace,
572 2017; Hudspeth, 1997). Mechanotransduction-mediated active hair bundle movements have been
573 reported in turtle and frog HCs (Benser et al., 1996; Crawford and Fettiplace, 1985; Denk and
574 Webb, 1992; Howard and Hudspeth, 1987; Martin et al., 2003). The functional significance of
575 kinociliary beating remains to be elucidated; however, the kinocilium may serve as an active,
576 force-generating component of the hair bundle. Because the kinocilium is connected to the tallest
577 stereocilia via kinocilial links, we speculate that kinociliary motility may dynamically modulate the
578 mechanical properties of the hair bundle or influence tip-link tension to prime transduction
579 channels. Kinociliary beating is sufficient to drive stereocilia bundle movement (Videos S1 and
580 S2). Even when constrained by the overlying otolithic membrane or cupula, changes in kinociliary
581 stiffness could still affect the bundle's mechanical dynamics. Importantly, such autonomous
582 rhythms are unlikely to disrupt temporally accurate encoding of head motion, as spontaneous
583 bundle movements driven by mechanotransduction have also been observed in bullfrog saccular
584 HCs (Benser et al., 1996; Martin et al., 2003). Moreover, auditory and vestibular afferent neurons
585 also generate spontaneous action potentials in both developing and mature animals. Although we
586 did not examine when spontaneous kinocilia beat emerges during development, our analysis
587 showed that key motile cilia signature genes and proteins are expressed at P2, suggesting that
588 spontaneous kinocilia beat may already be present at this age. Such activity may help refine HC
589 maturation and neural connections and prime the vestibular central pathway for its later function.

590 In summary, this study demonstrates that the kinocilium of vestibular HCs is a unique hybrid
591 cilium, exhibiting near-complete molecular features of both primary and motile cilia. While it shares
592 structural and molecular similarities with motile cilia and sperm flagella, it also possesses distinct
593 architectural and functional characteristics. Future investigations employing kinocilium-specific
594 proteomics, cryo-ET, and single-particle analysis will be critical for fully characterizing kinocilium
595 molecular composition and organization. Although kinocilia motility was observed in bullfrog and
596 mouse vestibular HCs in the present study, the functional significance of kinocilia motility remains
597 to be elucidated.
598
599 **MATERIALS AND METHODS**
600 Male and female CBA/J mice were purchased from the Jackson Laboratory (Stock #:000656)
601 and reared in Animal Care Facility of Creighton University and NIDCD. American bullfrogs (*Rana*
602 *catesbiana*) were purchased from Carolina Biological Supply Co. The animal usage and care were
603 approved by the Institutional Animal Care and Use Committees of Creighton University (Protocol
604 #1046.3) and NIDCD (NIDCD ACUC Protocol #1215).
605 *1. Cell dissociation, cDNA libraries preparation and RNA-Sequencing*
606 Male and female CBA/J mice aged 10 weeks were used for scRNA-seq. Cochlear and
607 vestibular end organs (utricle, saccule, and crista) were dissected from the inner ear and placed
608 in Petri dishes containing cold L-15 medium (Gibco; #11320033). After the cochlear and
609 vestibular sensory epithelia and neurons were dissected out, they were transferred into two
610 individual 1.5 ml tubes for enzymatic digestion (Collagenase IV from Sigma, concentration:
611 1mg/ml collagenase) in L-15 medium. After 10 minutes of incubation at room temperature, the
612 enzymatic solution was removed and replaced with 400 µl L-15 media containing 10% fetal bovine
613 serum. The tissues in two tubes were mechanically triturated by 200 µL Eppendorf pipette tips.
614 After that, the suspension containing cochlear and vestibular cells was then passed through 40
615 µm strainers for filtration and pelleted at 300 g for 5 mins. After removing extra media, cells were
616 then reconstituted in the 50 ul L-15 with 10% fetal bovine serum media and used for cDNA library
617 preparation. Seven mice were used for each biological replicate. Six biological replicates for
618 cochlear sensory epithelium and four biological replicates for vestibular sensory epithelia were
619 prepared for scRNA-seq.
620 The emulsion droplets were constructed using a 10x Genomics Controller device following
621 the manufacturer's instruction manual. cDNA libraries were constructed using the 10x Genomics
622 Chromium Single Cell 3' Reagent Kits V3.1. High Sensitivity DNA Kits (Agilent Technologies) were

623 used to perform quality control for each library in an Agilent 2100 Bioanalyzer. cDNA libraries
624 were sequenced in an Illumina NextSeq 6000 sequencer aiming for 240 billion 150 bp long paired-
625 end reads.

626 *2.Single-cell RNA-seq data process and analysis*

627 Raw transcriptomic datasets of adult cochlear and vestibular HCs from scRNA-seq have been
628 deposited to GEO (GSE283534). The FASTQ files were mapped to mm10 reference genome to
629 generate the single-cell expression matrices following the CellRanger count pipeline (version
630 6.1.2). The Cellranger output data was then processed with the Seurat package (version 4.3.0) in
631 R (version 4.1.3).

632 Genes expressed in at least ten cells were included in the analysis. Cells with numbers of
633 expressed genes <200 or >3,000 and cells with numbers of unique molecular identifiers (UMI) >
634 15,000 were filtered out. Cells with >20% mitochondrial genes were also excluded from the
635 analysis.

636 The gene expression data from individual samples were converted into a natural logarithm
637 and normalized under the same condition. Data from six cochlear and four vestibular replicates
638 were integrated separately based on the anchors identified from the top 2,000 highly variable
639 genes of individual normalized expression matrices. The Shared Nearest Neighbor graph method
640 can calculate the neighborhood overlap (Jaccard index) between every cell and its nearest
641 neighbors, which was used for cluster determination at a resolution of 0.6 on PCA-reduced
642 expression data for the top 30 principal components.

643 Clustering results for cochlear and vestibular datasets were visualized separately using t-
644 distributed stochastic neighbor embedding (t-SNE). Cluster annotations were initially produced
645 using SingleR and then corrected where appropriate based on well-known cellular markers for
646 cochlear and vestibular cells.

647 Entrez Gene, HGNC, OMIM, and Ensembl database were used for verification, reference, and
648 analyses. Online Databases of Ciliogenics (https://ciliogenics.com/), CiliaCarta
649 (https://ngdc.cncb.ac.cn/databasecommons/database/id/6383), and Primary Cilium Proteome
650 (https://esbl.nhlbi.nih.gov/Databases/CiliumProteome/) were also used for reference.

651 GO analysis in Fig. S1 was performed using ShinyGO 0.82 (Ge et al., 2020). The Venn
652 diagrams in Fig. 5B and Fig. S3 were generated using Venny 2.1
653 (https://bioinfogp.cnb.csic.es/tools/venny/), except for the sperm Venn diagram in Fig. S3E, which
654 was plotted using nVenn (https://degradome.uniovi.es/cgi-bin/nVenn/nvenn.cgi). Fig. 5C was

created with BioRender.com and further modified using Adobe Photoshop.

3. Immunocytochemistry

Inner ears were fixed overnight with 4% paraformaldehyde at 4°C. Cochlear and vestibular sensory epithelia were dissected out. After several washes with PBS, the tissue was blocked for 1 hour with 0.25% normal goat serum in PBS containing Triton-X-100 (0.01%) and goat serum (10%). Primary antibodies against DNM1 (AB3458, Abcam), SLC7A14 (HPA045929, Sigma), TJAP1 (NBP1-80902, Novus), FOXJ1 (14-9965-82, ThermoFisher), CCDC39 (HPA035364, Sigma), CCDC40 (PA5-54653, ThermoFisher), DNAH5 (31079-1-AP, ThermoFisher), DNAH6 (HPA036391, Sigma), TEKT1 (HPA044444, Millipore Sigma), CLUAP1 (PA5-83710, Thermo Fisher), IFT172 (28441-1-AP) and acetylated tubulin (T6793, Sigma) were incubated with the tissues for 12 hours at 4°C. After washes with PBS, secondary antibody (1:500) (Alexa fluor molecular probe 488 or 555; Invitrogen) was added and incubated for 2 hours at room temperature. Alexa Fluro™ 405 or 488 phalloidin (A30104 or A12379, Invitrogen) was used to label stereocilia bundles. Tissues were washed with PBS and mounted on glass microscopy slides with antifade solution (5 ml PBS, 5 ml glycerol, 0.1 g *n*-Propyl gallate). Images were captured using Nikon TI-2 Spinning Disk or Zeiss LSM 980 Inverted confocal microscope.

4. Single molecule fluorescence in situ hybridization

Single molecule fluorescence *in situ* hybridization was used to validate the expression of 15 genes in 10 µm-thin sections. Samples were prepared in formalin-fixed paraffin embedded tissue. Probes for 18 genes were purchased from ACD. These genes include *Adam11*, (580971), *Aqp11* (803751), *C1ql1* (465081), *Cdh23* (567261-C2), *Chrna10* (818521), *Cib2* (846681), *Cib3* (1105771), *Dnm3* (451841), *Ikzf2* (500001), *Kcnq4* (707481), *Otof* (485678), *Pcdh20* (467491), *Slc7a14* (544781), *Tmc1* (Cat No: 520911-C2) and *Tbx2* (448991-C2). Methods for the RNAscope™ 2.5 HD Assay from Advanced Cell Diagnostics were followed.

5. Electron microscopy

The mouse inner ears were fixed with 4% paraformaldehyde and 2.5% glutaraldehyde in 0.1 M sodium cacodylate buffer (pH 7.4) with 2 mM $CaCl_2$. The bullfrog crista ampullaris was fixed with 3% paraformaldehyde, 2% glutaraldehyde, 2% tannic acid and 0.5% calcium chloride in 0.1 M sodium cacodylate buffer (pH 6.8) with 0.1 mM $CaCl_2$ (Kachar et al., 1990). The tissues were then post-fixed for 1 hour with 1% OsO_4 in 0.1 M sodium cacodylate buffer and washed. For SEM, cochleae and vestibular tissues were dehydrated via an ethanol series, critical point dried from CO_2, and sputter-coated with platinum. The morphology of the HC stereocilia bundle was

687 examined in a FEI Quanta 200 scanning electron microscope and photographed. For TEM, the
688 bullfrog crista ampullaris was embedded in plastic (Epon 812 Epoxy Resin) after dehydration via
689 an ethanol series. 70-nm thin sections were cut with a diamond knife and collected on 300-mesh
690 grids. The thin section was post-stained with 3% uranyl acetate for 15 min and 1.5% lead citrate
691 for 3 min. The preparations were examined in an electron microscope (JEOL 100CX) and
692 photographed.

693 *6. Measurements of ciliary motion*

694 Bullfrogs were anesthetized with 20 μg/g of 3-aminobenzoic acid ethyl ester and decapitated.
695 The saccular macula was carefully dissected out under cooled frog's Ringer solution. The otoliths
696 were gently removed with forceps in fresh Ringer solution(Jaeger et al., 1994). The saccular
697 macula was placed under an Olympus upright microscope and kinocilia motility was visualized
698 using DIC and 60x objective and captured with a camera.

699 The Eustachian tube was dissected out from CBA/J mice and sectioned along its longitudinal
700 length. The preparation was bathed in L-15 medium (Invitrogen), containing 136 mM NaCl, 5.8
701 mM NaH_2PO_4, 5.4 mM KCl, 1.4 mM $CaCl_2$, 0.9 mM $MgCl_2$, 0.4 mM $MgSO_4$, and 10 mM HEPES-
702 NaOH (pH 7.4, 300 mmol/l) in an experimental chamber mounted on the stage of a Leica upright
703 microscope. Crista ampullaris was also dissected from 10-week-old CBA/J mice and bathed in L-
704 15 medium. The tissue was attached to the bottom of the chamber by the weight of two thin
705 platinum rods (0.5 mm in diameter). The tissue was mounted with the cilia or hair bundles facing
706 upward toward the water-immersion objective. The cilia and hair bundles were imaged using a
707 63x water immersion objective (Leica) and magnified by an additional 10x relay lens. Ciliary
708 motion was measured and calibrated by a photodiode-based measurement system mounted on
709 the Leica upright microscope (Jia and He, 2005). The magnified image of the hair bundle was
710 projected onto a photodiode through a rectangular slit. The image was positioned to one side of
711 the silt with 50% of the rectangular slit being covered by the magnified image of the bundle. Cilia
712 motion modulated the light influx to the photodiode. The photocurrent response was calibrated to
713 displacement units by moving the slit a fixed distance (0.5 μm) with the image of the cell in front
714 of the photodiode. After amplification, the photocurrent signal was low pass-filtered by an
715 antialiasing filter before being digitized by a 16-bit A/D board (Digidata 1550A; Molecular Devices).
716 The motile responses were low-pass filtered at 250 Hz and digitized at 1 kHz. Ciliary motion was
717 acquired in a two-second window for each trial and 20 trials were captured for each cell in one
718 recording. The power spectrum of the response was averaged and analyzed in the frequency

719 domain using Clampfit software (version 10, Molecular Devices). The experiments were
720 performed at room temperature (22±2°C).

721 *7. Predicted model of the 96-nm modular repeat in adult vestibular kinocilia*

722 The 96-nm repeat structures of the human respiratory axoneme (PDB: 8J07) and bovine
723 sperm flagellum (PDB: 9FQR) were used as structural references to model the vestibular kinocilia
724 axoneme. Candidate vestibular HC genes identified through transcriptomic profiling were
725 annotated and mapped to their respective axonemal compartments based on known or predicted
726 protein localizations within these reference structures. The 8J07 model lacked atomic modeling
727 for the full-length RS3 (Zhao et al., 2025), despite its presence in the corresponding cryo-EM
728 density map (EMD-35888), due to the uncharacterized proteome of RS3 in the human respiratory
729 system. To address this, RS3 components from the sperm axoneme structure (PDB: 9FQR)
730 excluding sperm-specific proteins were extracted, fitted into the EMD-35888 density using
731 ChimeraX's "fit-to-map" tool, and overlaid onto the 8J07 model to complete the RS3 architecture.
732 All structural visualization and model integration were performed using UCSF ChimeraX v1.6.
733 (Pettersen et al., 2021). In the models, DNAH5 and DNAH9 (present in our HC data) occupy the
734 ODA region in human respiratory cilia, while DNAH8 and DNAH17 occupy the same region in
735 sperm (but are not expressed in our dataset). Since they correspond structurally, we did not mark
736 them as missing in the sperm-based kinocilia model.

737
738
739

740 **FIGURE LEGEND**
741
742 **Fig. 1**: Single-cell transcriptional atlas of cochlear and vestibular cells. **A**: Schematic drawing of
743 the organ of Corti (top panel) and representative images of IHCs and OHCs from adult mouse
744 cochleae. **B**: Schematic drawing of the utricle (top panel) and confocal images of the utricle
745 prepared from an adult mouse. HCs are stained with MYO6, SOX2 and DAPI. SOX2-positive cells
746 include type II HCs and SCs underneath HCs. **C**: Representative images of type I and type II HCs
747 from utricular and saccular maculae as well as crista ampullaris from adult mice. **D**, **E**: tSNE plots
748 of distinct cell types detected in the adult CBA mouse cochlea (D) and utricle, saccule and crista.
749 Different cell types are color-coded. **F**: Feature plots of the expression 6 marker genes in different
750 HC populations. **G**: Dot plot heatmap of average expression and cellular detection rate of 28
751 representative marker genes in different HC types in cochleae and vestibular end organs.
752 Abbreviations: IHC (inner HC); OHC (outer HC); SGN (spiral ganglion neuron); SC (Schwann
753 cell)/SGC (satellite glial cell); DC (Deiters' cell)/PC (pillar cell); IPhC (inner phalangeal cell)/IB
754 (inner border cell); ISC (inner sulcus cell); HeC (Hensen's cell); SpC (spindle cell)/RC (root cell);
755 MC (marginal cell)/IC (intermediate cell); BaC (basal cell); MP (macrophage); RM (Reissner's
756 membrane); BC (B cell); TC (T cell); Gran (granulocyte); Mono (monocyte); RBC (red blood cell);
757 OSC (outer sulcus cell); TBC (tympanic border cell). Type I HC (type I HC); Type II HC (type II
758 HC); SESC (sensory epithelial SC); TEC (transitional epithelial cell); PTEC (peripheral transitional
759 epithelial cell); ERC (epithelial roof cell). Neurons (vestibular neurons). For those cells whose
760 definite identities cannot be annotated, the top expressed genes were used for identification and
761 annotation. These cells include Tectb$^+$, Mgp$^+$, Coch$^+$, Prl$^+$, Otos$^+$, Emilin2$^+$/Cavin2$^+$, Fxyd2$^+$/Kcnk2$^+$,
762 Prtn3$^+$/Ccl5$^+$, and Ptgds$^+$/Coch$^+$.
763
764 **Figure 2**: Similarity and difference among different HC types and biological processes enriched
765 in cochlear and vestibular HCs. **A**: PCA plot showing similarity based on pseudo bulk RNA-seq
766 data from four HC types. **B**: PCA plot showing similarity based on individual HC gene expression
767 among the four HC types. **C**: Venn diagram depicting the number of expressed genes (RPKM >
768 0) in four HC types. **D**: Volcano plot showing differentially expressed genes between different HC
769 types. Red dots indicate differentially expressed genes with P-value < 10^e-5 and $\log_2$ fold change
770 > 1. Only the top 20 differentially expressed genes are labeled. **E**: Biological processes enriched
771 in vestibular HCs compared to cochlear HCs. Biological processes related to motile cilia are
772 enriched. **F**: Biological processes enriched in type I HCs compared to type II HCs. **G**: Biological
773 processes enriched in type II HCs compared to type I HCs.
774
775 **Figure 3:** Shared and unique genes expressed in cochlear and vestibular HCs. **A**: Violin plots of
776 the expression 72 genes in four different HC types. **B**: Validation of differential expressions of 9
777 genes (with underline in **A**) in cochlear and vestibular HCs in thin section. Bar: 10 μm for all images
778 in B. **C**: Confocal images of expression of DNM1, SLC7A14, and TJAP1 in cochlear and vestibular
779 HCs. Bar: 10 μm for all images in C.
780
781 **Figure 4:** Expression of genes related to HC specialization. **A**: Heatmap showing expression of
782 genes related to stereocilia bundles, mechanotransduction, ion channels and synaptic structure.
783 **B**: Validation of gene expression using smFISH. Bar: 10 μm.
784
785 **Figure 5.** Cilia-related genes detected in cochlear and vestibular HCs. **A:** Schematic illustration
786 of HC hair bundle (adapted from Schwander et al., 2010). **B**: Venn diagram of the number of genes
787 in each database and the cilia-related genes detected in HC transcriptomes. **C**: Schematic

788 illustration of primary and motile cilia, highlighting 9+0 or 9+2 arrangement of microtubules for
789 primary and motile cilia, respectively: radial spokes (RS), central pair complex (CPC), nexin–
790 dynein regulatory complex (N-DRC), microtubule inner proteins (MIPs), inner and outer dynein
791 arms (IDA and ODA). **D**: Expression of top 50 cilia-related genes and genes related to IFT in the
792 four types of HCs. **E**: Immunostaining of IFT172 and CLUAP1 expression in vestibular kinocilia.
793 Bar: 5 µm. **F**: Violin plots showing aggregated expression of genes associated with 96-nm repeat.
794 Expression value of these genes is based on Supplementary Table 1. **G**: Heatmaps of comparison
795 of gene expressions related to motile-cilia machinery in cochlear and vestibular HCs. Red
796 asterisks indicate the genes whose encoded proteins are expressed in both cilia and cytoplasm
797 or are multifunctional.
798
799 **Figure 6**: Expression of motile cilia-related genes/proteins in the vestibular HCs. **A:** Expression of
800 motile cilia-related genes in zebrafish, mouse, and human vestibular HCs. Expression values of
801 these genes are based on Supplementary Table 1 (mouse), Data Citation 4 (zebrafish, Barta et
802 al., 2018), and Wang et al., 2024 (human). Mouse gene nomenclature is used in heatmaps. **B:**
803 Confocal images of the expression of key motile cilia-related proteins. Scale bars represent 5 µm.
804 **C**: SEM micrograph of hair bundles of OHCs from P2 cochlea. Kinocilia (in magenta) are still
805 present at this age. Bar: 2.5 µm. **D:** Comparison of expression of motile cilia-related genes
806 between P2 cochlear and vestibular HCs. Gene expression values are based on HC transcriptomic
807 dataset by Burns et al., 2015. Red asterisks mark the genes whose encoded proteins are
808 expressed in both cilia and cytoplasm or multifunctional. Red arrows indicate *Dnah5* and *Dnah6*,
809 which were not detected in P2 cochlear HCs. **E:** Confocal images of expression of CCDC39,
810 CCDC40 and DNAH6 in P2 vestibular and cochlear HCs. CCDC39, CCDC40, and DNAH6 were
811 not expressed in cochlear HCs at P2. Bar: 5 µm.
812
813 **Figure 7:** Kinocilia morphology and motility. **A**: TEM images of stereocilia and kinocilium from
814 bullfrog crista HCs. Different regions of the kinocilium in higher magnification are also shown.
815 Long black arrows indicate where the magnified images were taken. Bars: 250 nm. Red arrow
816 indicates two central microtubule singlets. Short black arrows mark absence of central
817 microtubule singlets in the distal regions near the tip of kinocilium and transition zone. **B**: Images
818 captured from *in vitro* live imaging of kinocilium and bundle motion of a bullfrog crista HC. The
819 images were captured at a speed of 15 frames per second. Black arrows indicate kinocilium. **C**:
820 Representative waveforms of spontaneous cilia motion from middle ear tissue. The FFT analysis
821 of cilia motion is also shown. **D:** Three representative waveforms of spontaneous motion of hair
822 bundles. The response waveform in blue was taken from a hair bundle with no spontaneous
823 motility. FFT analysis of bundle motion is shown. Response waveforms and spectra are color-
824 coded and -matched.
825
826 **Figure 8**: Predicted models of the molecular architecture of 96 nm axonemal repeat of vestibular
827 kinocilia. **A-B**: Longitudinal and cross-sectional views of the doublet microtubule and associated
828 structure in 96-nm repeat, derived from combining cryo-EM data and single-cell transcriptomic
829 analysis from human respiratory (A) and bovine sperm flagella (B). Key axonemal motile-
830 machinery components are color-coded: ODA (Indian red), IDA (cyan), N-DRC (green), MIPs
831 (orchid), RS (purple), and external coiled-coils (blue). Radial spoke 3 (RS3) has not been resolved
832 to atomic resolution, but its shorter form (RS3s) is depicted. Doublet microtubules (DMT) are
833 represented in gray. Regions highlighted in gold indicate the absence of corresponding transcripts
834 in our mouse transcriptomic data. **C**: Genes which are not detected in mouse and human
835 vestibular HC transcriptomes and related to motility-relevant compartments are listed in the table.

836 The roles of these genes in the 96-nm repeat module and cilia motility and ciliopathy are also
837 included.
838

REFERENCE

Andersen JS, Vijayakumaran A, Godbehere C, Lorentzen E, Mennella V, Schou KB. 2024. Uncovering structural themes across cilia microtubule inner proteins with implications for human cilia function. Nature Communications **15**:2687. DOI: https://doi.org/10.1038/s41467-024-46737-3

Anvarian Z, Mykytyn K, Mukhopadhyay S, Pedersen LB, Christensen ST. 2019. Cellular signalling by primary cilia in development, organ function and disease. Nature Reviews Nephrology **15**:199–219. DOI: https://doi.org/10.1038/s41581-019-0116-9

Assad JA, Shepherd GMG, Corey DP. 1991. Tip-link integrity and mechanical transduction in vertebrate hair cells. Neuron **7**:985–994. DOI: https://doi.org/10.1016/0896-6273(91)90343-X, PMID: 1764247

Baird RA. 1994. Comparative transduction mechanisms of hair cells in the bullfrog utriculus. II. Sensitivity and response dynamics to hair bundle displacement. Journal of Neurophysiology **71**:685–705. DOI: https://doi.org/10.1152/jn.1994.71.2.685

Barta CL, Liu H, Chen L, Giffen KP, Li Y, Kramer KL, Beisel KW, He DZ. 2018. RNA-seq transcriptomic analysis of adult zebrafish inner ear hair cells. Scientific Data **5**:180005. DOI: https://doi.org/10.1038/sdata.2018.5

Becker-Heck A, Zohn IE, Okabe N, Pollock A, Lenhart KB, Sullivan-Brown J, McSheene J, Loges NT, Olbrich H, Haeffner K, Fliegauf M, Horvath J, Reinhardt R, Nielsen KG, Marthin JK, Baktai G, Anderson KV, Geisler R, Niswander L, Omran H, Burdine RD. 2011. The coiled-coil domain containing protein CCDC40 is essential for motile cilia function and left-right axis formation. Nature Genetics **43**:79–84. DOI: https://doi.org/10.1038/ng.727

Benser ME, Marquis RE, Hudspeth AJ. 1996. Rapid, Active Hair Bundle Movements in Hair Cells from the Bullfrog's Sacculus. Journal of Neuroscience **16**:5629–5643. DOI: https://doi.org/10.1523/JNEUROSCI.16-18-05629.1996, PMID: 8795619

Brody SL, Pan J, Huang T, Xu J, Xu H, Koenitizer JR, Brennan SK, Nanjundappa R, Saba TG, Rumman N, Berical A, Hawkins FJ, Wang X, Zhang R, Mahjoub MR, Horani A, Dutcher SK. 2025. Undocking of an extensive ciliary network induces proteostasis and cell fate switching resulting in severe primary ciliary dyskinesia. Science Translational Medicine **17**:eadp5173. DOI: https://doi.org/10.1126/scitranslmed.adp5173

Brown A, Leung MR, Zeev-Ben-Mordehai T, Zhang R. 2025. TRiC Is a Structural Component of Mammalian Sperm Axonemes. Cytoskeleton (Hoboken, N.J.). DOI: https://doi.org/10.1002/cm.22005, PMID: 39927553

Brownell WE, Bader CR, Bertrand D, de Ribaupierre Y. 1985. Evoked mechanical responses of isolated cochlear outer hair cells. Science (New York, N.Y.) **227**:194–196. DOI: https://doi.org/10.1126/science.3966153, PMID: 3966153

Burns J, Stone J. 2017. Development and regeneration of vestibular hair cells in mammals. Seminars in cell & developmental biology **65**:96–105. DOI: https://doi.org/10.1016/j.semcdb.2016.11.001, PMID: 27864084

Burns JC, Kelly MC, Hoa M, Morell RJ, Kelley MW. 2015. Single-cell RNA-Seq resolves cellular complexity in sensory organs from the neonatal inner ear. Nature Communications **6**:8557. DOI: https://doi.org/10.1038/ncomms9557

Chen Z, Shiozaki M, Haas KM, Skinner WM, Zhao S, Guo C, Polacco BJ, Yu Z, Krogan NJ, Lishko PV, Kaake RM, Vale RD, Agard DA. 2023. De novo protein identification in mammalian sperm using in situ cryoelectron tomography and AlphaFold2 docking. Cell **186**:5041-5053.e19. DOI: https://doi.org/10.1016/j.cell.2023.09.017, PMID: 37865089

Choksi SP, Lauter G, Swoboda P, Roy S. 2014. Switching on cilia: transcriptional networks regulating ciliogenesis. Development **141**:1427–1441. DOI: https://doi.org/10.1242/dev.074666

Crawford AC, Fettiplace R. 1985. The mechanical properties of ciliary bundles of turtle cochlear hair cells. The Journal of Physiology **364**:359–379. DOI: https://doi.org/10.1113/jphysiol.1985.sp015750

Dallos P. 1992. The active cochlea. Journal of Neuroscience **12**:4575–4585. DOI: https://doi.org/10.1523/JNEUROSCI.12-12-04575.1992, PMID: 1464757

Dallos P, Wu X, Cheatham MA, Gao J, Zheng J, Anderson CT, Jia S, Wang X, Cheng WHY, Sengupta S, He DZZ, Zuo J. 2008. Prestin-Based Outer Hair Cell Motility Is Necessary for Mammalian Cochlear Amplification. Neuron **58**:333–339. DOI: https://doi.org/10.1016/j.neuron.2008.02.028

Dam TJP van, Kennedy J, Lee R van der, Vrieze E de, Wunderlich KA, Rix S, Dougherty GW, Lambacher NJ, Li C, Jensen VL, Leroux MR, Hjeij R, Horn N, Texier Y, Wissinger Y, Reeuwijk J van, Wheway G, Knapp B, Scheel JF, Franco B, Mans DA, Wijk E van, Képès F, Slaats GG, Toedt G, Kremer H, Omran H, Szymanska K, Koutroumpas K, Ueffing M, Nguyen T-MT, Letteboer SJF, Oud MM, Beersum SEC van, Schmidts M, Beales PL, Lu Q, Giles RH, Szklarczyk R, Russell RB, Gibson TJ, Johnson CA, Blacque OE, Wolfrum U, Boldt K, Roepman R, Hernandez-Hernandez V, Huynen MA. 2019. CiliaCarta: An integrated

and validated compendium of ciliary genes. PLOS ONE **14**:e0216705. DOI: https://doi.org/10.1371/journal.pone.0216705

Denk W, Webb WW. 1992. Forward and reverse transduction at the limit of sensitivity studied by correlating electrical and mechanical fluctuations in frog saccular hair cells. Hearing Research **60**:89–102. DOI: https://doi.org/10.1016/0378-5955(92)90062-R

Eatock RA, Rüsch A, Lysakowski A, Saeki M. 1998. Hair Cells in Mammalian Utricles. Otolaryngology–Head and Neck Surgery **119**:172–181. DOI: https://doi.org/10.1016/S0194-5998(98)70052-X

Eatock RA, Songer JE. 2011. Vestibular Hair Cells and Afferents: Two Channels for Head Motion Signals. Annual Review of Neuroscience **34**:501–534. DOI: https://doi.org/10.1146/annurev-neuro-061010-113710

Erickson T, Biggers WP, Williams K, Butland SE, Venuto A. 2023. Regionalized Protein Localization Domains in the Zebrafish Hair Cell Kinocilium. Journal of Developmental Biology **11**:28. DOI: https://doi.org/10.3390/jdb11020028

Fawcett DW, Ito S. 1965. The fine structure of bat spermatozoa. American Journal of Anatomy **116**:567–609. DOI: https://doi.org/10.1002/aja.1001160306

Fettiplace R. 2017. Hair Cell Transduction, Tuning, and Synaptic Transmission in the Mammalian Cochlea. Comprehensive Physiology **7**:1197–1227. DOI: https://doi.org/10.1002/cphy.c160049, PMID: 28915323

Flock Å, Flock B, Murray E. 1977. Studies on the Sensory Hairs of Receptor Cells in the Inner Ear. Acta Oto-Laryngologica **83**:85–91. DOI: https://doi.org/10.3109/00016487709128817, PMID: 842331

Ge SX, Jung D, Yao R. 2020. ShinyGO: a graphical gene-set enrichment tool for animals and plants. Bioinformatics **36**:2628–2629. DOI: https://doi.org/10.1093/bioinformatics/btz931

Giese APJ, Tang Y-Q, Sinha GP, Bowl MR, Goldring AC, Parker A, Freeman MJ, Brown SDM, Riazuddin S, Fettiplace R, Schafer WR, Frolenkov GI, Ahmed ZM. 2017. CIB2 interacts with TMC1 and TMC2 and is essential for mechanotransduction in auditory hair cells. Nature Communications **8**:43. DOI: https://doi.org/10.1038/s41467-017-00061-1

Gillespie PG, Müller U. 2009. Mechanotransduction by Hair Cells: Models, Molecules, and Mechanisms. Cell **139**:33–44. DOI: https://doi.org/10.1016/j.cell.2009.09.010, PMID: 19804752

Gui M, Farley H, Anujan P, Anderson JR, Maxwell DW, Whitchurch JB, Botsch JJ, Qiu T, Meleppattu S, Singh SK, Zhang Q, Thompson J, Lucas JS, Bingle CD, Norris DP, Roy S, Brown A. 2021. *De novo* identification of mammalian ciliary motility proteins using cryo-EM. Cell **184**:5791-5806.e19. DOI: https://doi.org/10.1016/j.cell.2021.10.007

Hansen JN, Sun H, Kahnert K, Westenius E, Johannesson A, Tzavlaki K, Winsnes C, Pohjanen E, Fall J, Navarro FB, Bäckström A, Lindskog C, Johansson F, Von Feilitzen K, Vega AD, Uhlén M, Casals AM, Mahdessian D, Lindstrand A, Axelsson U, Lundberg E. 2024. Intrinsic Diversity In Primary Cilia Revealed Through Spatial Proteomics. DOI: https://doi.org/10.1101/2024.10.20.619273

Hansen JN, Sun H, Kahnert K, Westenius E, Johannesson A, Villegas C, Le T, Tzavlaki K, Winsnes C, Pohjanen E, Mäkiniemi A, Fall J, Navarro FB, Bäckström A, Lindskog C, Johansson F, Feilitzen K von, Delgado-Vega AM, Casals AM, Mahdessian D, Uhlén M, Sheu S-H, Lindstrand A, Axelsson U, Lundberg E. 2025. Intrinsic heterogeneity of primary cilia revealed through spatial proteomics. Cell **188**:6804-6824.e16. DOI: https://doi.org/10.1016/j.cell.2025.08.039, PMID: 41005307

He DZZ, Dallos P. 1999. Development of Acetylcholine-Induced Responses in Neonatal Gerbil Outer Hair Cells. Journal of Neurophysiology **81**:1162–1170. DOI: https://doi.org/10.1152/jn.1999.81.3.1162

Hong J, Lee C, Papoulas O, Pan J, Takagishi M, Manzi N, Dickinson DJ, Horani A, Brody SL, Marcotte E, Park TJ, Wallingford JB. 2025. Molecular organization of the distal tip of vertebrate motile cilia. DOI: https://doi.org/10.1101/2025.02.19.639145

Howard J, Hudspeth AJ. 1987. Mechanical relaxation of the hair bundle mediates adaptation in mechanoelectrical transduction by the bullfrog's saccular hair cell. Proceedings of the National Academy of Sciences **84**:3064–3068. DOI: https://doi.org/10.1073/pnas.84.9.3064

Hudspeth A. 1997. Mechanical amplification of stimuli by hair cells. Current Opinion in Neurobiology **7**:480–486. DOI: https://doi.org/10.1016/s0959-4388(97)80026-8, PMID: 9287199

Jaeger RG, Fex J, Kachar B. 1994. Structural basis for mechanical transduction in the frog vestibular sensory apparatus: II. The role of microtubules in the organization of the cuticular plate. Hearing Research **77**:207–215. DOI: https://doi.org/10.1016/0378-5955(94)90268-2, PMID: 7928733

Jan TA, Eltawil Y, Ling AH, Chen L, Ellwanger DC, Heller S, Cheng AG. 2021. Spatiotemporal dynamics of inner ear sensory and non-sensory cells revealed by single-cell transcriptomics. Cell Reports **36**:109358. DOI: https://doi.org/10.1016/j.celrep.2021.109358, PMID: 34260939

Jen H-I, Hill MC, Tao L, Sheng K, Cao W, Zhang H, Yu HV, Llamas J, Zong C, Martin JF, Segil N, Groves AK. 2019. Transcriptomic and epigenetic regulation of hair cell regeneration in the mouse utricle and its potentiation by Atoh1. eLife **8**:e44328. DOI: https://doi.org/10.7554/eLife.44328

Jia S, Dallos P, He DZZ. 2007. Mechanoelectric Transduction of Adult Inner Hair Cells. Journal of Neuroscience **27**:1006–1014. DOI: https://doi.org/10.1523/JNEUROSCI.5452-06.2007, PMID: 17267554

Jia S, He DZZ. 2005. Motility-associated hair-bundle motion in mammalian outer hair cells. Nature Neuroscience **8**:1028–1034. DOI: https://doi.org/10.1038/nn1509

Kachar B, Brownell WE, Altschuler R, Fex J. 1986. Electrokinetic shape changes of cochlear outer hair cells. Nature **322**:365–368. DOI: https://doi.org/10.1038/322365a0

Kachar B, Parakkal M, Fex J. 1990. Structural basis for mechanical transduction in the frog vestibular sensory apparatus: I. The otolithic membrane. Hearing Research **45**:179–190. DOI: https://doi.org/10.1016/0378-5955(90)90119-A

Kachar B, Parakkal M, Kurc M, Zhao Y, Gillespie PG. 2000. High-resolution structure of hair-cell tip links. Proceedings of the National Academy of Sciences **97**:13336–13341. DOI: https://doi.org/10.1073/pnas.97.24.13336

Kikuchi T, Takasaka T, Tonosaki A, Watanabe H. 1989. Fine structure of guinea pig vestibular kinocilium. Acta Oto-Laryngologica **108**:26–30. DOI: https://doi.org/10.3109/00016488909107388, PMID: 2527457

Kindt KS, Finch G, Nicolson T. 2012. Kinocilia Mediate Mechanosensitivity in Developing Zebrafish Hair Cells. Developmental Cell **23**:329–341. DOI: https://doi.org/10.1016/j.devcel.2012.05.022

Lagziel A, Ahmed ZM, Schultz JM, Morell RJ, Belyantseva IA, Friedman TB. 2005. Spatiotemporal pattern and isoforms of cadherin 23 in wild type and *waltzer* mice during inner ear hair cell development. Developmental Biology **280**:295–306. DOI: https://doi.org/10.1016/j.ydbio.2005.01.015

Lechtreck K-F, Gould TJ, Witman GB. 2013. Flagellar central pair assembly in Chlamydomonas reinhardtii. Cilia **2**:15. DOI: https://doi.org/10.1186/2046-2530-2-15

Legal T, Joachimiak E, Parra M, Peng W, Tam A, Black C, Valente-Paterno M, Brouhard G, Gaertig J, Wloga D, Bui KH. 2024. Structure of the ciliary tip central pair reveals the unique role of the microtubule-seam binding protein SPEF1. DOI: https://doi.org/10.1101/2024.12.02.626492

Legal T, Parra M, Tong M, Black CS, Joachimiak E, Valente-Paterno M, Lechtreck K, Gaertig J, Bui KH. 2023. CEP104/FAP256 and associated cap complex maintain stability of the ciliary tip. Journal of Cell Biology **222**:e202301129. DOI: https://doi.org/10.1083/jcb.202301129

Leibovici M, Verpy E, Goodyear RJ, Zwaenepoel I, Blanchard S, Lainé S, Richardson GP, Petit C. 2005. Initial characterization of kinocilin, a protein of the hair cell kinocilium. Hearing Research **203**:144–153. DOI: https://doi.org/10.1016/j.heares.2004.12.002

Leung MR, Sun C, Zeng J, Anderson JR, Niu Q, Huang W, Noteborn WEM, Brown A, Zeev-Ben-Mordehai T, Zhang R. 2025. Structural diversity of axonemes across mammalian motile cilia. Nature 1–8. DOI: https://doi.org/10.1038/s41586-024-08337-5

Li A, Xue J, Peterson EH. 2008. Architecture of the Mouse Utricle: Macular Organization and Hair Bundle Heights. Journal of Neurophysiology **99**:718–733. DOI: https://doi.org/10.1152/jn.00831.2007

Li Y, Liu H, Giffen KP, Chen L, Beisel KW, He DZZ. 2018. Transcriptomes of cochlear inner and outer hair cells from adult mice. Scientific Data **5**:180199. DOI: https://doi.org/10.1038/sdata.2018.199

Liberman MC, Gao J, He DZZ, Wu X, Jia S, Zuo J. 2002. Prestin is required for electromotility of the outer hair cell and for the cochlear amplifier. **419**:5.

Liu H, Pecka JL, Zhang Q, Soukup GA, Beisel KW, He DZZ. 2014. Characterization of Transcriptomes of Cochlear Inner and Outer Hair Cells. Journal of Neuroscience **34**:11085–11095. DOI: https://doi.org/10.1523/JNEUROSCI.1690-14.2014, PMID: 25122905

Lysakowski A, Goldberg JM. 1997. A regional ultrastructural analysis of the cellular and synaptic architecture in the chinchilla cristae ampullares. Journal of Comparative Neurology **389**:419–443. DOI: https://doi.org/10.1002/(SICI)1096-9861(19971222)389:3%253C419::AID-CNE5%253E3.0.CO;2-3

Ma Y, He J, Li S, Yao D, Huang C, Wu J, Lei M. 2023. Structural insight into the intraflagellar transport complex IFT-A and its assembly in the anterograde IFT train. Nature Communications **14**:1506. DOI: https://doi.org/10.1038/s41467-023-37208-2

Martin P, Bozovic D, Choe Y, Hudspeth AJ. 2003. Spontaneous Oscillation by Hair Bundles of the Bullfrog's Sacculus. Journal of Neuroscience **23**:4533–4548. DOI: https://doi.org/10.1523/JNEUROSCI.23-11-04533.2003, PMID: 12805294

McInturff S, Burns JC, Kelley MW. 2018. Characterization of spatial and temporal development of Type I and Type II hair cells in the mouse utricle using new cell-type-specific markers. Biology Open **7**:bio038083. DOI: https://doi.org/10.1242/bio.038083

Meng G-Q, Wang Y, Luo C, Tan Y-M, Li Y, Tan C, Tu C, Zhang Q-J, Hu L, Zhang H, Meng L-L, Liu C-Y, Deng L, Lu G-X, Lin G, Du J, Tan Y-Q, Sha Y, Wang L, He W-B. 2024. Bi-allelic variants in DNAH3 cause male infertility with asthenoteratozoospermia in humans and mice. Human Reproduction Open **2024**:hoae003. DOI: https://doi.org/10.1093/hropen/hoae003, PMID: 38312775

Meng X, Li L, Lin C, Zhu Y, Feng Y, Zhou X, Tong Y, Wang S, Yin G, Liu R, Sun F, Yan X, Zhu X, Cong Y. 2024. Chaperonin TRiC bridges radial spokes for folding proteins locally translated in mammalian sperm flagella. DOI: https://doi.org/10.1101/2024.11.19.624414

Merveille A-C, Davis EE, Becker-Heck A, Legendre M, Amirav I, Bataille G, Belmont J, Beydon N, Billen F, Clément A, Clercx C, Coste A, Crosbie R, de Blic J, Deleuze S, Duquesnoy P, Escalier D, Escudier E, Fliegauf M, Horvath J, Hill K, Jorissen M, Just J, Kispert A, Lathrop M, Loges NT, Marthin JK, Momozawa Y, Montantin G, Nielsen KG, Olbrich H, Papon J-F, Rayet I, Roger G, Schmidts M, Tenreiro H, Towbin JA, Zelenika D, Zentgraf H, Georges M, Lequarré A-S, Katsanis N, Omran H, Amselem S. 2011. CCDC39 is required for assembly of inner dynein arms and the dynein regulatory complex and for normal ciliary motility in humans and dogs. Nature Genetics **43**:72–78. DOI: https://doi.org/10.1038/ng.726

Moon K-H, Ma J-H, Min H, Koo H, Kim H, Ko HW, Bok J. 2020. Dysregulation of sonic hedgehog signaling causes hearing loss in ciliopathy mouse models. eLife **9**:e56551. DOI: https://doi.org/10.7554/eLife.56551

Nagel ZD, Margulies CM, Chaim IA, McRee SK, Mazzucato P, Ahmad A, Abo RP, Butty VL, Forget AL, Samson LD. 2014. Multiplexed DNA repair assays for multiple lesions and multiple doses via transcription inhibition and transcriptional mutagenesis. Proceedings of the National Academy of Sciences **111**:E1823–E1832. DOI: https://doi.org/10.1073/pnas.1401182111

Oda T, Yanagisawa H, Kamiya R, Kikkawa M. 2014. A molecular ruler determines the repeat length in eukaryotic cilia and flagella. Science **346**:857–860. DOI: https://doi.org/10.1126/science.1260214

O'Donnell J, Zheng J. 2022. Vestibular Hair Cells Require CAMSAP3, a Microtubule Minus-End Regulator, for Formation of Normal Kinocilia. Frontiers in Cellular Neuroscience **16**:876805. DOI: https://doi.org/10.3389/fncel.2022.876805, PMID: 35783105

Pettersen EF, Goddard TD, Huang CC, Meng EC, Couch GS, Croll TI, Morris JH, Ferrin TE. 2021. UCSF ChimeraX: Structure visualization for researchers, educators, and developers. Protein Science **30**:70–82. DOI: https://doi.org/10.1002/pro.3943

Pir MS, Begar E, Yenisert F, Demirci HC, Korkmaz ME, Karaman A, Tsiropoulou S, Firat-Karalar EN, Blacque OE, Oner SS, Doluca O, Cevik S, Kaplan OI. 2024. CilioGenics: an integrated method and database for predicting novel ciliary genes. Nucleic Acids Research **52**:8127–8145. DOI: https://doi.org/10.1093/nar/gkae554

Polino AJ, Sviben S, Melena I, Piston DW, Hughes JW. 2023. Scanning electron microscopy of human islet cilia. Proceedings of the National Academy of Sciences **120**:e2302624120. DOI: https://doi.org/10.1073/pnas.2302624120

Pujol R, Pickett SB, Nguyen TB, Stone JS. 2014. Large basolateral processes on type II hair cells comprise a novel processing unit in mammalian vestibular organs. The Journal of comparative neurology **522**:3141–3159. DOI: https://doi.org/10.1002/cne.23625, PMID: 24825750

Ranum PT, Goodwin AT, Yoshimura H, Kolbe DL, Walls WD, Koh J-Y, He DZZ, Smith RJH. 2019. Insights into the Biology of Hearing and Deafness Revealed by Single-Cell RNA Sequencing. Cell Reports **26**:3160-3171.e3. DOI: https://doi.org/10.1016/j.celrep.2019.02.053

Riazuddin Saima, Belyantseva IA, Giese APJ, Lee K, Indzhykulian AA, Nandamuri SP, Yousaf R, Sinha GP, Lee S, Terrell D, Hegde RS, Ali RA, Anwar S, Andrade-Elizondo PB, Sirmaci A, Parise LV, Basit S, Wali A, Ayub M, Ansar M, Ahmad W, Khan SN, Akram J, Tekin M, Riazuddin Sheikh, Cook T, Buschbeck EK, Frolenkov GI, Leal SM, Friedman TB, Ahmed ZM. 2012. Alterations of the CIB2 calcium- and integrin-binding protein cause Usher syndrome type 1J and nonsyndromic deafness DFNB48. Nature Genetics **44**:1265–1271. DOI: https://doi.org/10.1038/ng.2426

Ricci AJ, Crawford AC, Fettiplace R. 2003. Tonotopic Variation in the Conductance of the Hair Cell Mechanotransducer Channel. Neuron **40**:983–990. DOI: https://doi.org/10.1016/S0896-6273(03)00721-9

Ricci AJ, Rennie KJ, Cochran SL, Kevetter GA, Correia MJ. 1997. Vestibular type I and type II hair cells. 1: Morphometric identification in the pigeon and gerbil. Journal of Vestibular Research: Equilibrium & Orientation **7**:393–406. PMID: 9376913

1060 Rüsch A, Thurm U. 1990. Spontaneous and electrically induced movements of ampullary kinocilia and stereovilli.
1061 Hearing Research **48**:247–263. DOI: https://doi.org/10.1016/0378-5955(90)90065-W
1062 Schwander M, Kachar B, Müller U. 2010. The cell biology of hearing. Journal of Cell Biology **190**:9–20. DOI:
1063 https://doi.org/10.1083/jcb.201001138
1064 Shi H, Wang H, Zhang C, Lu Y, Yao J, Chen Z, Xing G, Wei Q, Cao X. 2022. Mutations in OSBPL2 cause hearing
1065 loss associated with primary cilia defects via sonic hedgehog signaling. DOI:
1066 https://doi.org/10.1172/jci.insight.149626
1067 Shin J-B, Krey JF, Hassan A, Metlagel Z, Tauscher AN, Pagana JM, Sherman NE, Jeffery ED, Spinelli KJ, Zhao H,
1068 Wilmarth PA, Choi D, David LL, Auer M, Barr-Gillespie PG. 2013. Molecular architecture of the chick
1069 vestibular hair bundle. Nature Neuroscience **16**:365–374. DOI: https://doi.org/10.1038/nn.3312
1070 Silver IA, Erecińska M. 1997. Energetic demands of the Na+/K+ ATPase in mammalian astrocytes. Glia **21**:35–45.
1071 DOI: https://doi.org/10.1002/(SICI)1098-1136(199709)21:1%253C35::AID-GLIA4%253E3.0.CO;2-0
1072 Spoon C, Grant W. 2011. Biomechanics of hair cell kinocilia: experimental measurement of kinocilium shaft
1073 stiffness and base rotational stiffness with Euler–Bernoulli and Timoshenko beam analysis. Journal of
1074 Experimental Biology **214**:862–870. DOI: https://doi.org/10.1242/jeb.051151
1075 Stooke-Vaughan GA, Huang P, Hammond KL, Schier AF, Whitfield TT. 2012. The role of hair cells, cilia and
1076 ciliary motility in otolith formation in the zebrafish otic vesicle. Development **139**:1777–1787. DOI:
1077 https://doi.org/10.1242/dev.079947
1078 Sung YH, Baek I-J, Kim YH, Gho YS, Oh SP, Lee YJ, Lee H-W. 2016. PIERCE1 is critical for specification of left-
1079 right asymmetry in mice. Scientific Reports **6**:27932. DOI: https://doi.org/10.1038/srep27932
1080 Tai L, Yin G, Huang X, Sun F, Zhu Y. 2023. In-cell structural insight into the stability of sperm microtubule
1081 doublet. Cell Discovery **9**:1–19. DOI: https://doi.org/10.1038/s41421-023-00606-3
1082 Tian X, Zhao H, Zhou J. 2023. Organization, functions, and mechanisms of the BBSome in development,
1083 ciliopathies, and beyond. eLife **12**:e87623. DOI: https://doi.org/10.7554/eLife.87623
1084 Vasquez SSV, van Dam J, Wheway G. 2021. An updated SYSCILIA gold standard (SCGSv2) of known ciliary
1085 genes, revealing the vast progress that has been made in the cilia research field. Molecular Biology of the
1086 Cell **32**:br13. DOI: https://doi.org/10.1091/mbc.E21-05-0226
1087 Walton T, Gui M, Velkova S, Fassad MR, Hirst RA, Haarman E, O'Callaghan C, Bottier M, Burgoyne T, Mitchison
1088 HM, Brown A. 2023. Axonemal structures reveal mechanoregulatory and disease mechanisms. Nature
1089 **618**:625–633. DOI: https://doi.org/10.1038/s41586-023-06140-2
1090 Wang D, Zhou J. 2021. The Kinocilia of Cochlear Hair Cells: Structures, Functions, and Diseases. Frontiers in Cell
1091 and Developmental Biology **9**. DOI: https://doi.org/10.3389/fcell.2021.715037
1092 Wang T, Ling AH, Billings SE, Hosseini DK, Vaisbuch Y, Kim GS, Atkinson PJ, Sayyid ZN, Aaron KA, Wagh D,
1093 Pham N, Scheibinger M, Zhou R, Ishiyama A, Moore LS, Maria PS, Blevins NH, Jackler RK, Alyono JC,
1094 Kveton J, Navaratnam D, Heller S, Lopez IA, Grillet N, Jan TA, Cheng AG. 2024. Single-cell
1095 transcriptomic atlas reveals increased regeneration in diseased human inner ear balance organs. Nature
1096 Communications **15**:4833. DOI: https://doi.org/10.1038/s41467-024-48491-y
1097 Wang X, Liu S, Cheng Q, Qu C, Ren R, Du H, Li N, Yan K, Wang Y, Xiong W, Xu Z. 2023. CIB2 and CIB3
1098 Regulate Stereocilia Maintenance and Mechanoelectrical Transduction in Mouse Vestibular Hair Cells.
1099 Journal of Neuroscience **43**:3219–3231. DOI: https://doi.org/10.1523/JNEUROSCI.1807-22.2023, PMID:
1100 37001993
1101 Wilkerson BA, Zebroski HL, Finkbeiner CR, Chitsazan AD, Beach KE, Sen N, Zhang RC, Bermingham-McDonogh
1102 O. 2021. Novel cell types and developmental lineages revealed by single-cell RNA-seq analysis of the
1103 mouse crista ampullaris. eLife **10**:e60108. DOI: https://doi.org/10.7554/eLife.60108
1104 Wu D, Freund JB, Fraser SE, Vermot J. 2011. Mechanistic Basis of Otolith Formation during Teleost Inner Ear
1105 Development. Developmental Cell **20**:271–278. DOI: https://doi.org/10.1016/j.devcel.2010.12.006, PMID:
1106 21316594
1107 Xia X, Shimogawa MM, Wang H, Liu S, Wijono A, Langousis G, Kassem AM, Wohlschlegel JA, Hill KL, Zhou
1108 ZH. 2025. Trypanosome doublet microtubule structures reveal flagellum assembly and motility
1109 mechanisms. Science **387**:eadr3314. DOI: https://doi.org/10.1126/science.adr3314
1110 Yamamoto R, Song K, Yanagisawa H, Fox L, Yagi T, Wirschell M, Hirono M, Kamiya R, Nicastro D, Sale WS.
1111 2013. The MIA complex is a conserved and novel dynein regulator essential for normal ciliary motility.
1112 Journal of Cell Biology **201**:263–278. DOI: https://doi.org/10.1083/jcb.201211048
1113 Yang M, Hussain HMJ, Khan M, Muhammad Z, Zhou J, Ma A, Huang X, Ye J, Chen M, Zhi A, Liu T, Khan R, Ali
1114 A, Shah W, Zeb A, Ahmad N, Zhang H, Xu B, Ma H, Shi Q, Shi B. 2024. Deficiency in a special dynein

DNAH12 causes male infertility by impairing DNAH1 and DNALI1 recruitment in humans and mice. eLife **13**. DOI: https://doi.org/10.7554/eLife.100350.1

Zhao Y, Song K, Tavakoli A, Gui L, Fernandez-Gonzalez A, Zhang S, Dzeja PP, Mitsialis SA, Zhang X, Nicastro D. 2025. Mouse radial spoke 3 is a metabolic and regulatory hub in cilia. Nature Structural & Molecular Biology **32**:1542–1554. DOI: https://doi.org/10.1038/s41594-025-01594-6

Zheng J, Shen W, He DZZ, Long KB, Madison LD, Dallos P. 2000. Prestin is the motor protein of cochlear outer hair cells. Nature **405**:149–155. DOI: https://doi.org/10.1038/35012009

Acknowledgments

We acknowledge the use of the Auditory and Vestibular Technology (AVT) Core of Translational Hearing Research Center at Creighton University for high-resolution confocal imaging and library preparation (10x Genomics), and the University of Nebraska DNA Sequencing Core Facility for scRNA-seq. The AVT core at Creighton University receives partial support from NIH grant 1P20GM139762-01 from NIGMS. The University of Nebraska DNA Sequencing Core receives partial support from the NCRR (RR018788). Scanning electron microscope was acquired through a Nebraska EPSCoR MRI award (Creighton-Department of Chemistry & Biochemistry) and was wholly funded by Nebraska EPSCoR. This research was supported by the NIDCD/NIH Intramural Research Program funds Z01-DC000002 to BK and AT and utilized the computational resources of the NIH HPC Biowulf cluster (http://hpc.nih.gov).

Funding:

National Institutes of Health grant IRP funds Z01-DC000002 from NIDCD (BK and AT)
National Institutes of Health grant R01 DC016807 from NIDCD (DH)

Author contributions: D.H., B.K., and A.T. conceived the project. Z.X., H.L., S.T., Y.L., and D.H. collected the inner ear tissues and prepared the library for scRNA-seq. Z.X., A.T., S.K., C.B., J.Z., L.T., and D.H. performed the bioinformatics analyses. A.T. conducted structural modeling. A.T., H.L., S.K., D.H., and B.K. carried out morphological and physiological experiments. A.T., Z.X., S.K., C.B., B.K., and D.H. contributed to the preparation and editing of the manuscript and figures.

Data and materials availability: Original scRNA-seq data are available (GSE283534). Data are visualized in the main text and the supplemental materials.

Supplemental files include:

Fig. S1: GO analysis of enriched genes in cellular localization and biological processes primarily related to cilia organization, assembly, maintenance, intracellular transport, and microtubule dynamics particularly associated with motile cilia
Fig. S2: Primary cilia-related genes in four HC types
Fig. S3: Comparison of HC transcriptomes with multi-tissue proteomics datasets
Fig. S4: ATAC-seq data indicating enhanced accessibility of motile-cilia machinery-associated gene loci in adult vestibular HCs
Fig. S5: Microtubule inner proteins and microtubule-associated proteins absent from mouse HC scRNA-seq data

Table S1: Transcriptomes of four HC types

Table S2: Genes/Gene products candidates associated with axonemal components in vestibular kinocilia derived from the 96-nm repeat structures of the human respiratory axoneme (PDB: 8J07). Missing genes in mouse vestibular hair cells are in red

Videos S1 and S2: Bullfrog kinocilia motility

Videos S3 and S4: Predicted structures models of molecular composition of the vestibular kinocilium based on the structural frameworks derived from human (video S3) respiratory (PDB: 8J07) (Walton et al., 2023) and bovine (video S4) sperm (PDB: 9FQR)(Leung et al., 2025) axonemes.

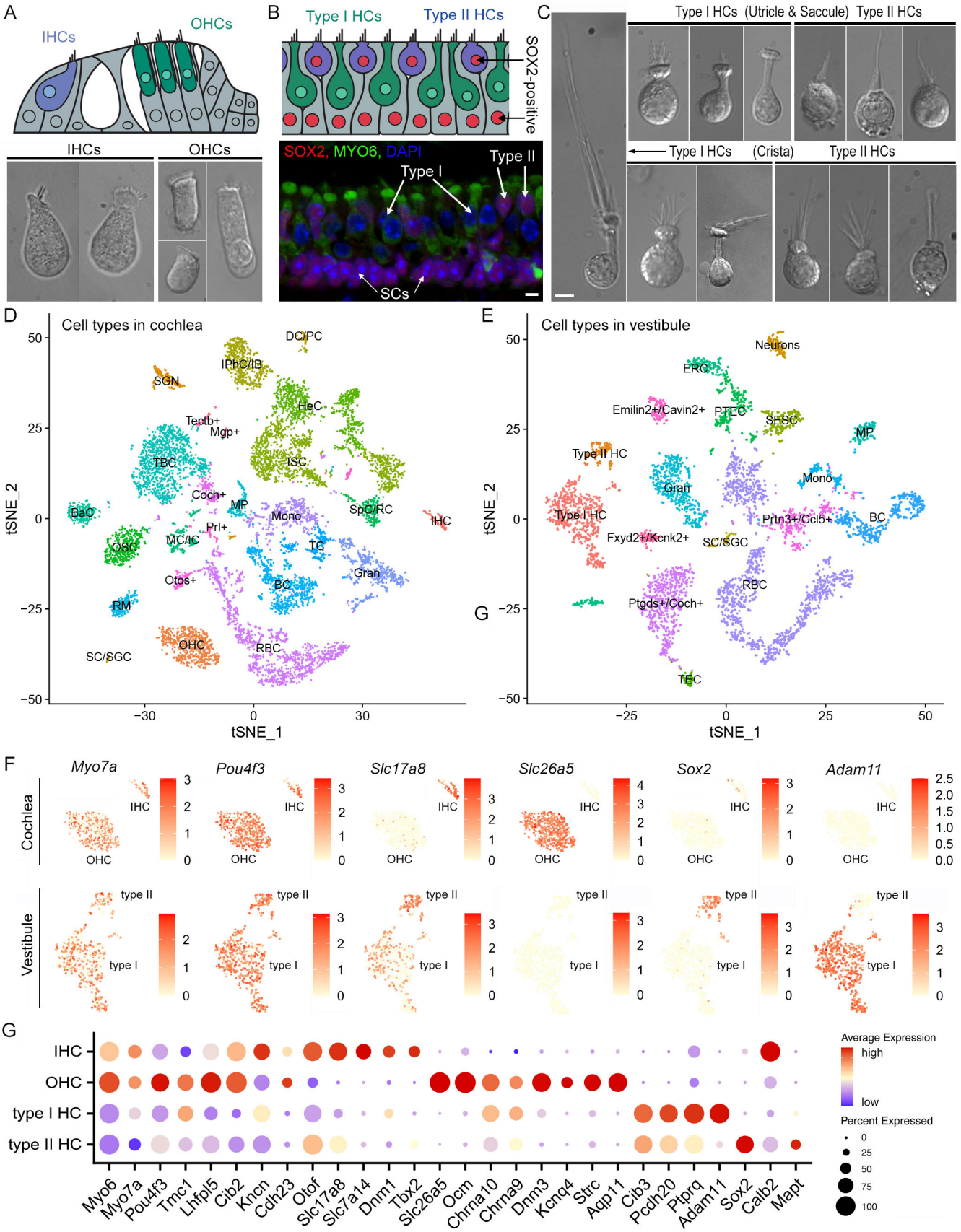
A
IHCs
OHCs
IHCs
OHCs
B
Type I HCs
Type II HCs
SOX2-positive
SOX2, MYO6, DAPI
Type I
Type II
SCs
C
Type I HCs (Utricle & Saccule) Type II HCs
Type I HCs (Crista) Type II HCs
D
Cell types in cochlea
tSNE_1
tSNE_2
DC/PC
IPhC/IB
SGN
HeC
Tectb+
Mgp+
TBC
ISC
Coch+
MP
Mono
SpC/RC
IHC
BaC
Prl+
MC/IC
OSC
TC
Gran
Otos+
BC
RM
OHC
RBC
SC/SGC
E
Cell types in vestibule
Neurons
ERC
Emilin2+/Cavin2+
PTEC
SESC
MP
Type II HC
Gran
Mono
Type I HC
Prtn3+/Ccl5+
BC
Fxyd2+/Kcnk2+
SC/SGC
RBC
Ptgds+/Coch+
TEC
F
Myo7a
Pou4f3
Slc17a8
Slc26a5
Sox2
Adam11
Cochlea
Vestibule
IHC
OHC
type II
type I
G
IHC
OHC
type I HC
type II HC
Myo6
Myo7a
Pou4f3
Tmc1
Lhfpl5
Cib2
Kncn
Cdh23
Otof
Slc17a8
Slc7a14
Dnm1
Tbx2
Slc26a5
Ocm
Chrna10
Chrna9
Dnm3
Kcnq4
Strc
Aqp11
Cib3
Pcdh20
Ptprq
Adam11
Sox2
Calb2
Mapt
Average Expression
high
low
Percent Expressed
0
25
50
75
100

Figure 1

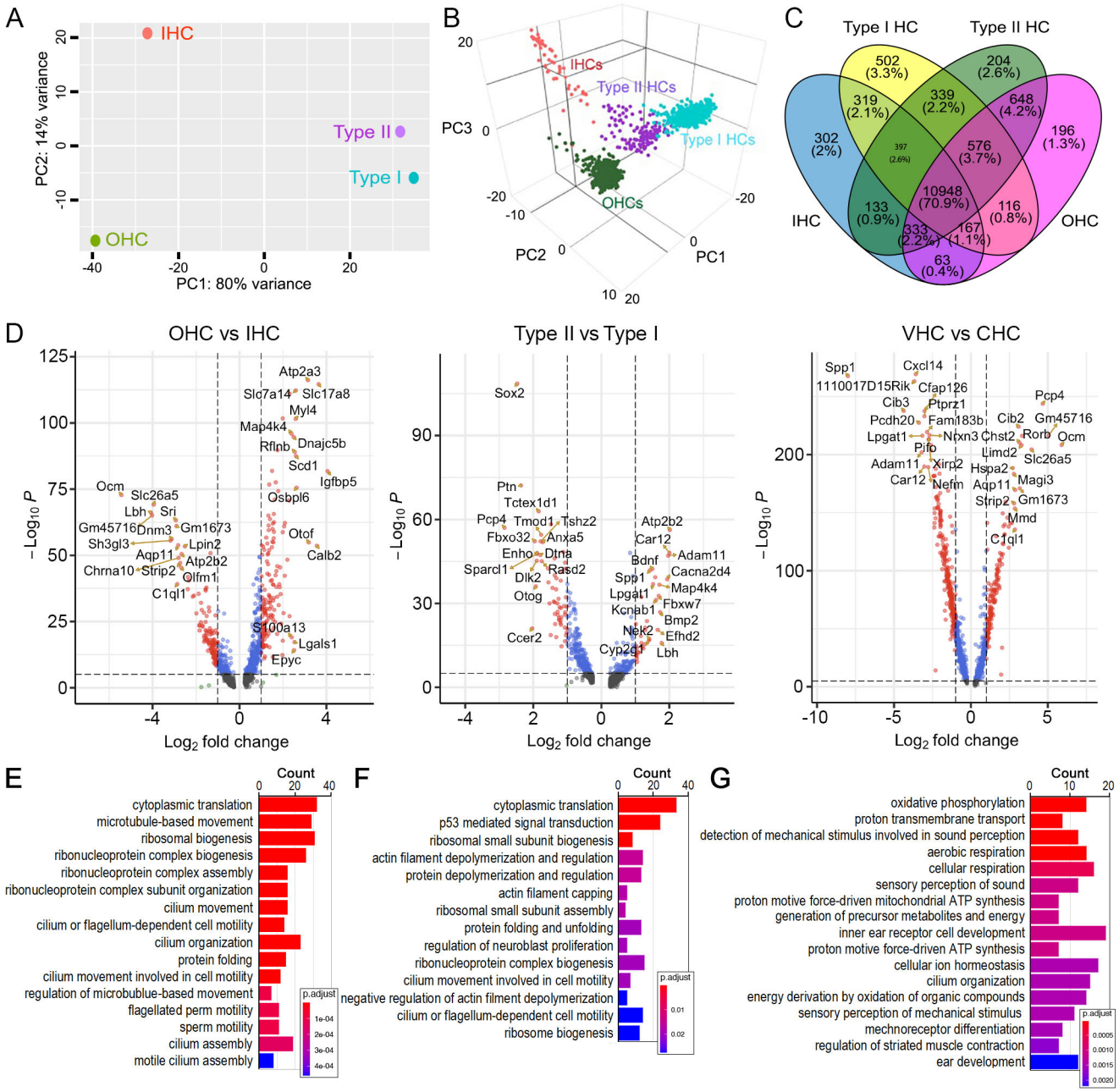
A
IHC
Type II
Type I
OHC
PC2: 14% variance
PC1: 80% variance
B
IHCs
Type II HCs
Type I HCs
OHCs
PC3
PC2
PC1
C
Type I HC
Type II HC
IHC
OHC
502 (3.3%)
204 (2.6%)
319 (2.1%)
339 (2.2%)
648 (4.2%)
302 (2%)
397 (2.6%)
576 (3.7%)
196 (1.3%)
10948 (70.9%)
133 (0.9%)
116 (0.8%)
333 (2.2%)
167 (1.1%)
63 (0.4%)
D
OHC vs IHC
Type II vs Type I
VHC vs CHC
– Log10 P
Log2 fold change
E
F
G
Count
cytoplasmic translation
microtubule-based movement
ribosomal biogenesis
ribonucleoprotein complex biogenesis
ribonucleoprotein complex assembly
ribonucleoprotein complex subunit organization
cilium movement
cilium or flagellum-dependent cell motility
cilium organization
protein folding
cilium movement involved in cell motility
regulation of microbublue-based movement
flagellated perm motility
sperm motility
cilium assembly
motile cilium assembly
p53 mediated signal transduction
ribosomal small subunit biogenesis
actin filament depolymerization and regulation
protein depolymerization and regulation
actin filament capping
ribosomal small subunit assembly
protein folding and unfolding
regulation of neuroblast proliferation
ribonucleoprotein complex biogenesis
cilium movement involved in cell motility
negative regulation of actin filment depolymerization
cilium or flagellum-dependent cell motility
ribosome biogenesis
oxidative phosphorylation
proton transmembrane transport
detection of mechanical stimulus involved in sound perception
aerobic respiration
cellular respiration
sensory perception of sound
proton motive force-driven mitochondrial ATP synthesis
generation of precursor metabolites and energy
inner ear receptor cell development
proton motive force-driven ATP synthesis
cellular ion homeostasis
cilium organization
energy derivation by oxidation of organic compounds
sensory perception of mechanical stimulus
mechnoreceptor differentiation
regulation of striated muscle contraction
ear development
p.adjust

Figure 2

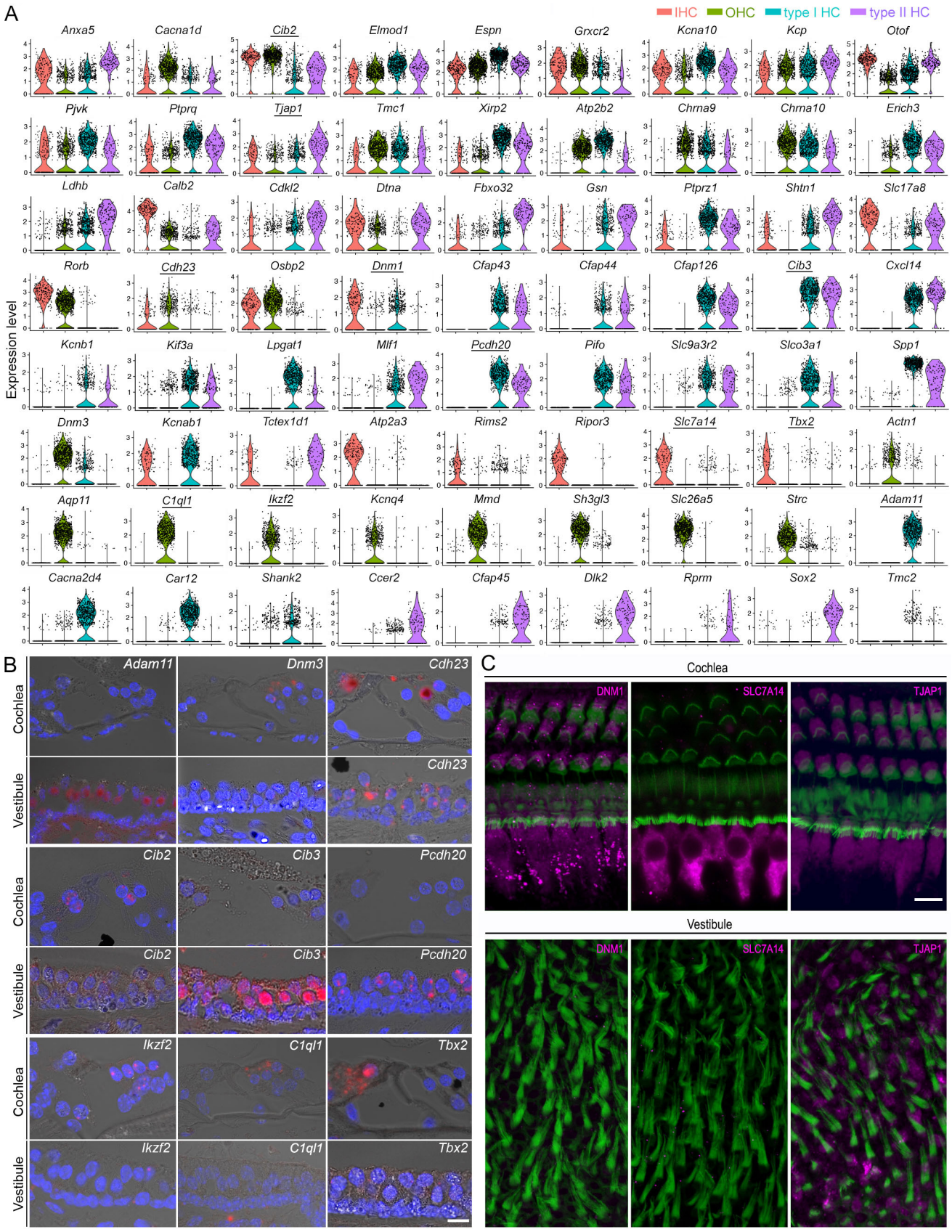
A
IHC
OHC
type I HC
type II HC
Expression level
Anxa5
Cacna1d
Cib2
Elmod1
Espn
Grxcr2
Kcna10
Kcp
Otof
Pjvk
Ptprq
Tjap1
Tmc1
Xirp2
Atp2b2
Chrna9
Chrna10
Erich3
Ldhb
Calb2
Cdkl2
Dtna
Fbxo32
Gsn
Ptprz1
Shtn1
Slc17a8
Rorb
Cdh23
Osbp2
Dnm1
Cfap43
Cfap44
Cfap126
Cib3
Cxcl14
Kcnb1
Kif3a
Lpgat1
Mlf1
Pcdh20
Pifo
Slc9a3r2
Slco3a1
Spp1
Dnm3
Kcnab1
Tctex1d1
Atp2a3
Rims2
Ripor3
Slc7a14
Tbx2
Actn1
Aqp11
C1ql1
Ikzf2
Kcnq4
Mmd
Sh3gl3
Slc26a5
Strc
Adam11
Cacna2d4
Car12
Shank2
Ccer2
Cfap45
Dlk2
Rprm
Sox2
Tmc2
B
Cochlea
Vestibule
Adam11
Dnm3
Cdh23
Cib2
Cib3
Pcdh20
Ikzf2
C1ql1
Tbx2
C
Cochlea
Vestibule
DNM1
SLC7A14
TJAP1

Figure 3

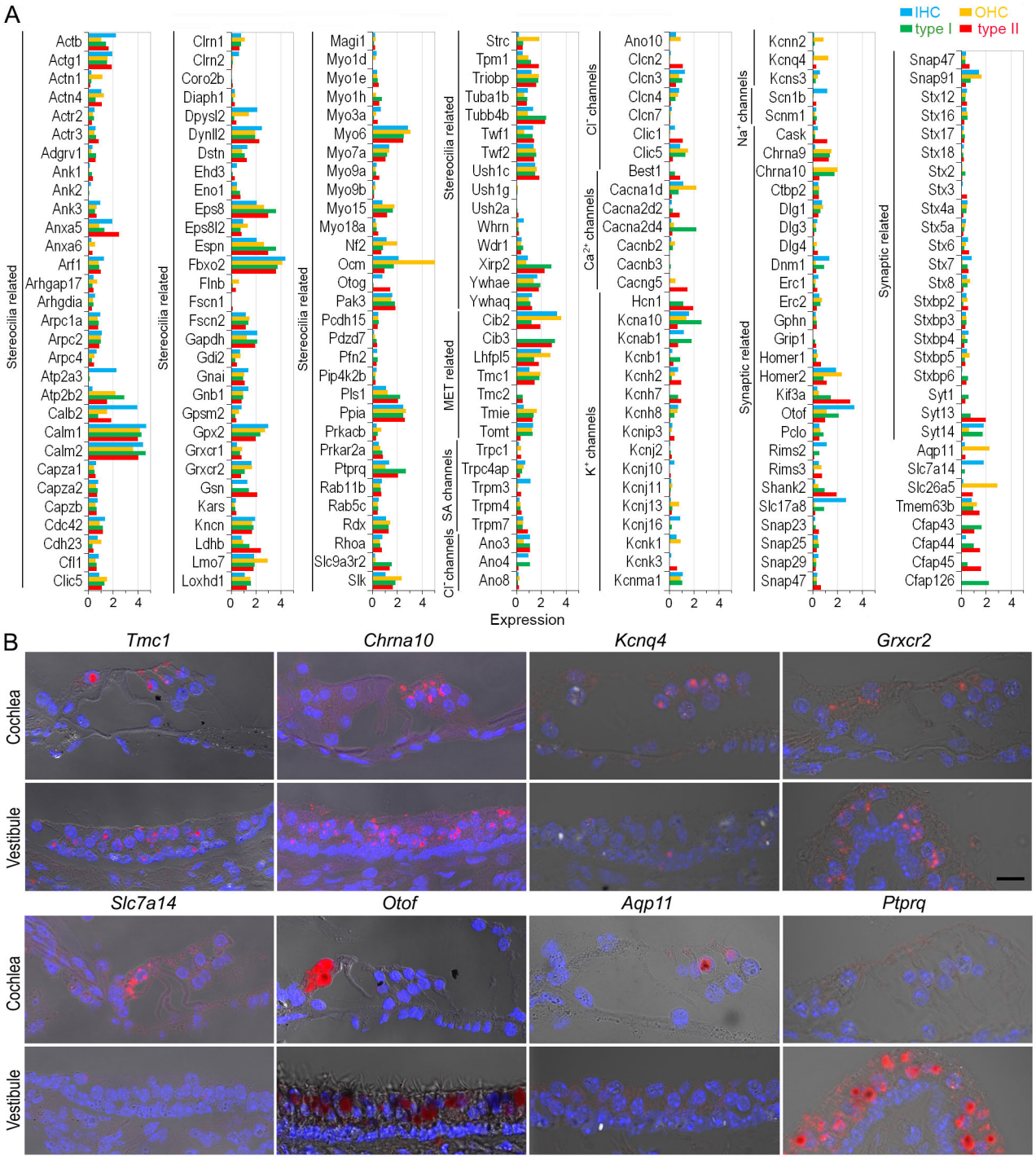
A
IHC
OHC
type I
type II
Stereocilia related
Actb
Actg1
Actn1
Actn4
Actr2
Actr3
Adgrv1
Ank1
Ank2
Ank3
Anxa5
Anxa6
Arf1
Arhgap17
Arhgdia
Arpc1a
Arpc2
Arpc4
Atp2a3
Atp2b2
Calb2
Calm1
Calm2
Capza1
Capza2
Capzb
Cdc42
Cdh23
Cfl1
Clic5
Clrn1
Clrn2
Coro2b
Diaph1
Dpysl2
Dynll2
Dstn
Ehd3
Eno1
Eps8
Eps8l2
Espn
Fbxo2
Flnb
Fscn1
Fscn2
Gapdh
Gdi2
Gnai
Gnb1
Gpsm2
Gpx2
Grxcr1
Grxcr2
Gsn
Kars
Kncn
Ldhb
Lmo7
Loxhd1
Magi1
Myo1d
Myo1e
Myo1h
Myo3a
Myo6
Myo7a
Myo9a
Myo9b
Myo15
Myo18a
Nf2
Ocm
Otog
Pak3
Pcdh15
Pdzd7
Pfn2
Pip4k2b
Pls1
Ppia
Prkacb
Prkar2a
Ptprq
Rab11b
Rab5c
Rdx
Rhoa
Slc9a3r2
Slk
Stereocilia related
Strc
Tpm1
Triobp
Tuba1b
Tubb4b
Twf1
Twf2
Ush1c
Ush1g
Ush2a
Whrn
Wdr1
Xirp2
Ywhae
Ywhaq
MET related
Cib2
Cib3
Lhfpl5
Tmc1
Tmc2
Tmie
Tomt
SA channels
Trpc1
Trpc4ap
Trpm3
Trpm4
Trpm7
Cl⁻ channels
Ano3
Ano4
Ano8
Cl⁻ channels
Ano10
Clcn2
Clcn3
Clcn4
Clcn7
Clic1
Clic5
Best1
Ca²⁺ channels
Cacna1d
Cacna2d2
Cacna2d4
Cacnb2
Cacnb3
Cacng5
K⁺ channels
Hcn1
Kcna10
Kcnab1
Kcnb1
Kcnh2
Kcnh7
Kcnh8
Kcnip3
Kcnj2
Kcnj10
Kcnj11
Kcnj13
Kcnj16
Kcnk1
Kcnk3
Kcnma1
Na⁺ channels
Kcnn2
Kcnq4
Kcns3
Scn1b
Scnm1
Cask
Chrna9
Chrna10
Ctbp2
Dlg1
Dlg3
Dlg4
Dnm1
Erc1
Erc2
Gphn
Grip1
Homer1
Homer2
Kif3a
Otof
Pclo
Rims2
Rims3
Shank2
Slc17a8
Snap23
Snap25
Snap29
Snap47
Synaptic related
Snap47
Snap91
Stx12
Stx16
Stx17
Stx18
Stx2
Stx3
Stx4a
Stx5a
Stx6
Stx7
Stx8
Stxbp2
Stxbp3
Stxbp4
Stxbp5
Stxbp6
Syt1
Syt13
Syt14
Aqp11
Slc7a14
Slc26a5
Tmem63b
Cfap43
Cfap44
Cfap45
Cfap126
0 2 4
Expression
B
Tmc1
Chrna10
Kcnq4
Grxcr2
Cochlea
Vestibule
Slc7a14
Otof
Aqp11
Ptprq
Cochlea
Vestibule

Figure 4

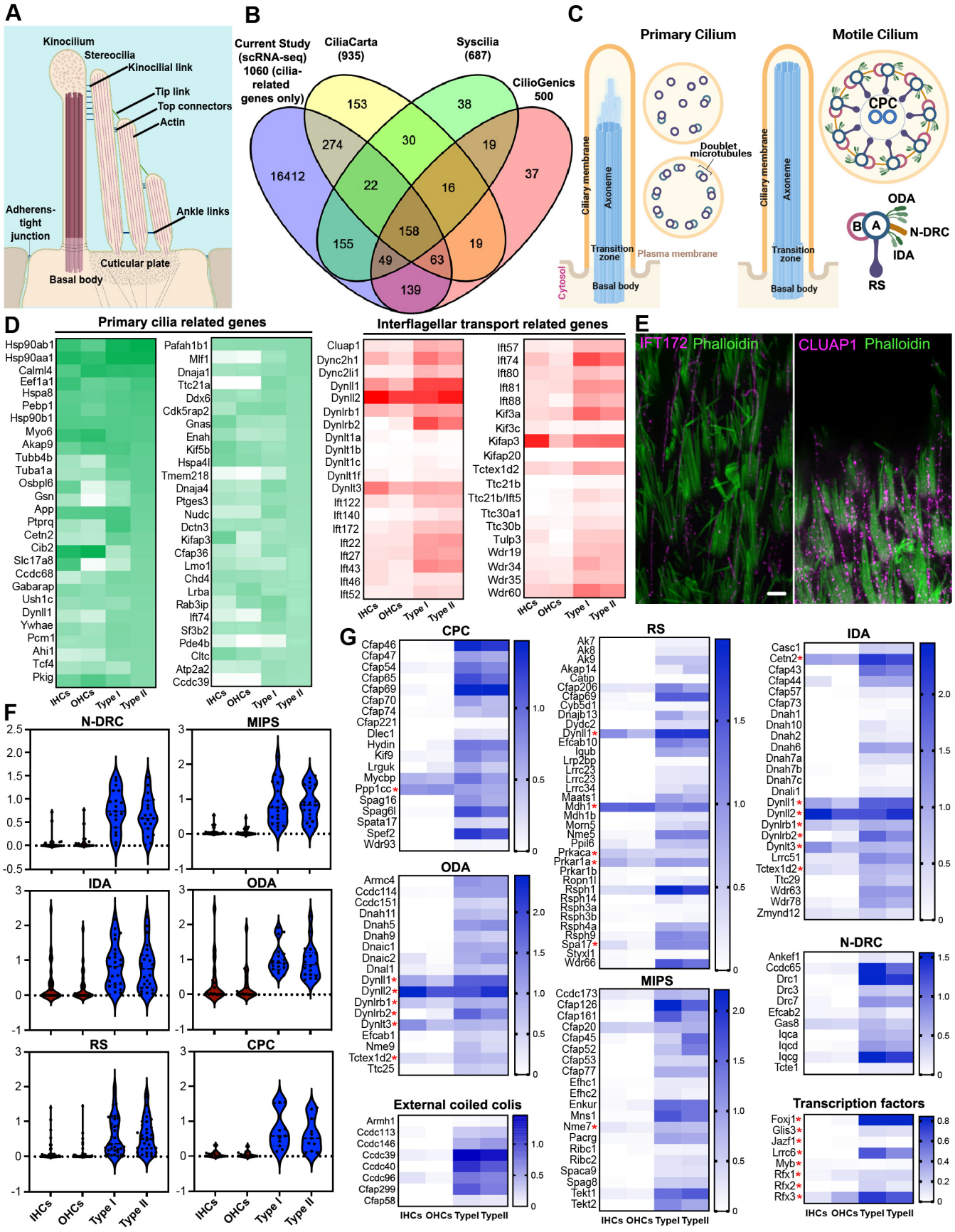
A
Kinocilium
Stereocilia
Kinocilial link
Tip link
Top connectors
Actin
Adherens-tight junction
Ankle links
Cuticular plate
Basal body
B
Current Study (scRNA-seq) 1060 (cilia-related genes only)
CiliaCarta (935)
Syscilia (687)
CilioGenics 500
16412
153
38
37
274
30
19
22
16
158
155
19
49
63
139
C
Primary Cilium
Motile Cilium
Ciliary membrane
Axoneme
Transition zone
Basal body
Cytosol
Plasma membrane
Doublet microtubules
CPC
ODA
N-DRC
IDA
RS
D
Primary cilia related genes
Interflagellar transport related genes
IHCs
OHCs
Type I
Type II
E
IFT172 Phalloidin
CLUAP1 Phalloidin
F
N-DRC
MIPS
IDA
ODA
RS
CPC
G
CPC
RS
IDA
ODA
N-DRC
MIPS
External coiled colis
Transcription factors
IHCs OHCs TypeI TypeII

Figure 5

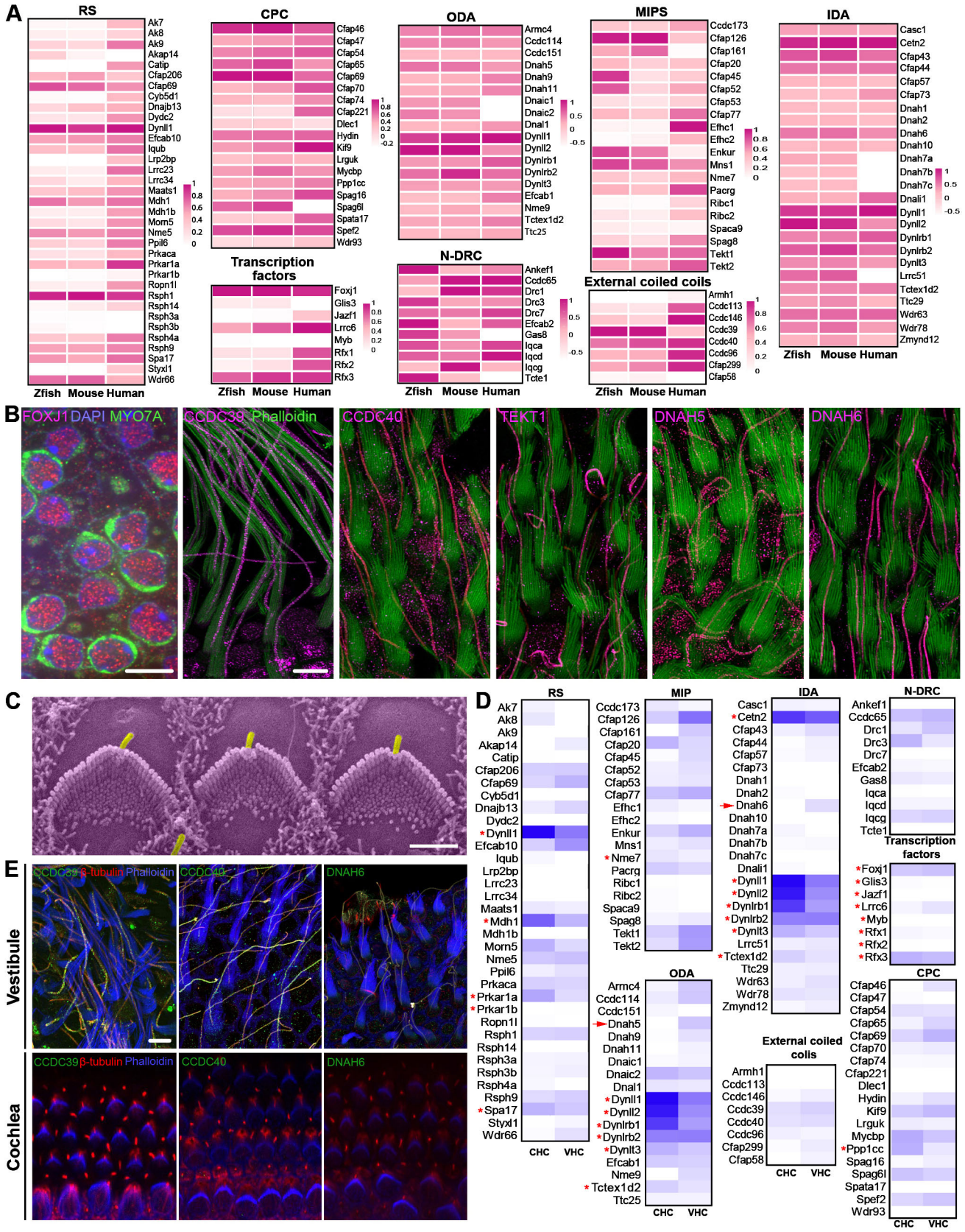
A
RS
Ak7
Ak8
Ak9
Akap14
Catip
Cfap206
Cfap69
Cyb5d1
Dnajb13
Dydc2
Dynll1
Efcab10
Iqub
Lrp2bp
Lrrc23
Lrrc34
Maats1
Mdh1
Mdh1b
Morn5
Nme5
Ppil6
Prkaca
Prkar1a
Prkar1b
Ropn1l
Rsph1
Rsph14
Rsph3a
Rsph3b
Rsph4a
Rsph9
Spa17
Styxl1
Wdr66
Zfish Mouse Human
CPC
Cfap46
Cfap47
Cfap54
Cfap65
Cfap69
Cfap70
Cfap74
Cfap221
Dlec1
Hydin
Kif9
Lrguk
Mycbp
Ppp1cc
Spag16
Spag6l
Spata17
Spef2
Wdr93
Zfish Mouse Human
ODA
Armc4
Ccdc114
Ccdc151
Dnah5
Dnah9
Dnah11
Dnaic1
Dnaic2
Dnal1
Dynll1
Dynll2
Dynlrb1
Dynlrb2
Dynlt3
Efcab1
Nme9
Tctex1d2
Ttc25
Zfish Mouse Human
MIPS
Ccdc173
Cfap126
Cfap161
Cfap20
Cfap45
Cfap52
Cfap53
Cfap77
Efhc1
Efhc2
Enkur
Mns1
Nme7
Pacrg
Ribc1
Ribc2
Spaca9
Spag8
Tekt1
Tekt2
Zfish Mouse Human
IDA
Casc1
Cetn2
Cfap43
Cfap44
Cfap57
Cfap73
Dnah1
Dnah2
Dnah6
Dnah10
Dnah7a
Dnah7b
Dnah7c
Dnali1
Dynll1
Dynll2
Dynlrb1
Dynlrb2
Dynlt3
Lrrc51
Tctex1d2
Ttc29
Wdr63
Wdr78
Zmynd12
Zfish Mouse Human
Transcription factors
Foxj1
Glis3
Jazf1
Lrrc6
Myb
Rfx1
Rfx2
Rfx3
Zfish Mouse Human
N-DRC
Ankef1
Ccdc65
Drc1
Drc3
Drc7
Efcab2
Gas8
Iqca
Iqcd
Iqcg
Tcte1
Zfish Mouse Human
External coiled coils
Armh1
Ccdc113
Ccdc146
Ccdc39
Ccdc40
Ccdc96
Cfap299
Cfap58
Zfish Mouse Human
B
FOXJ1 DAPI MYO7A
CCDC39 Phalloidin
CCDC40
TEKT1
DNAH5
DNAH6
C
E
Vestibule
Cochlea
CCDC39 β-tubulin Phalloidin
CCDC40
DNAH6
D
RS
MIP
IDA
N-DRC
ODA
Transcription factors
CPC
External coiled colis
CHC VHC

Figure 6

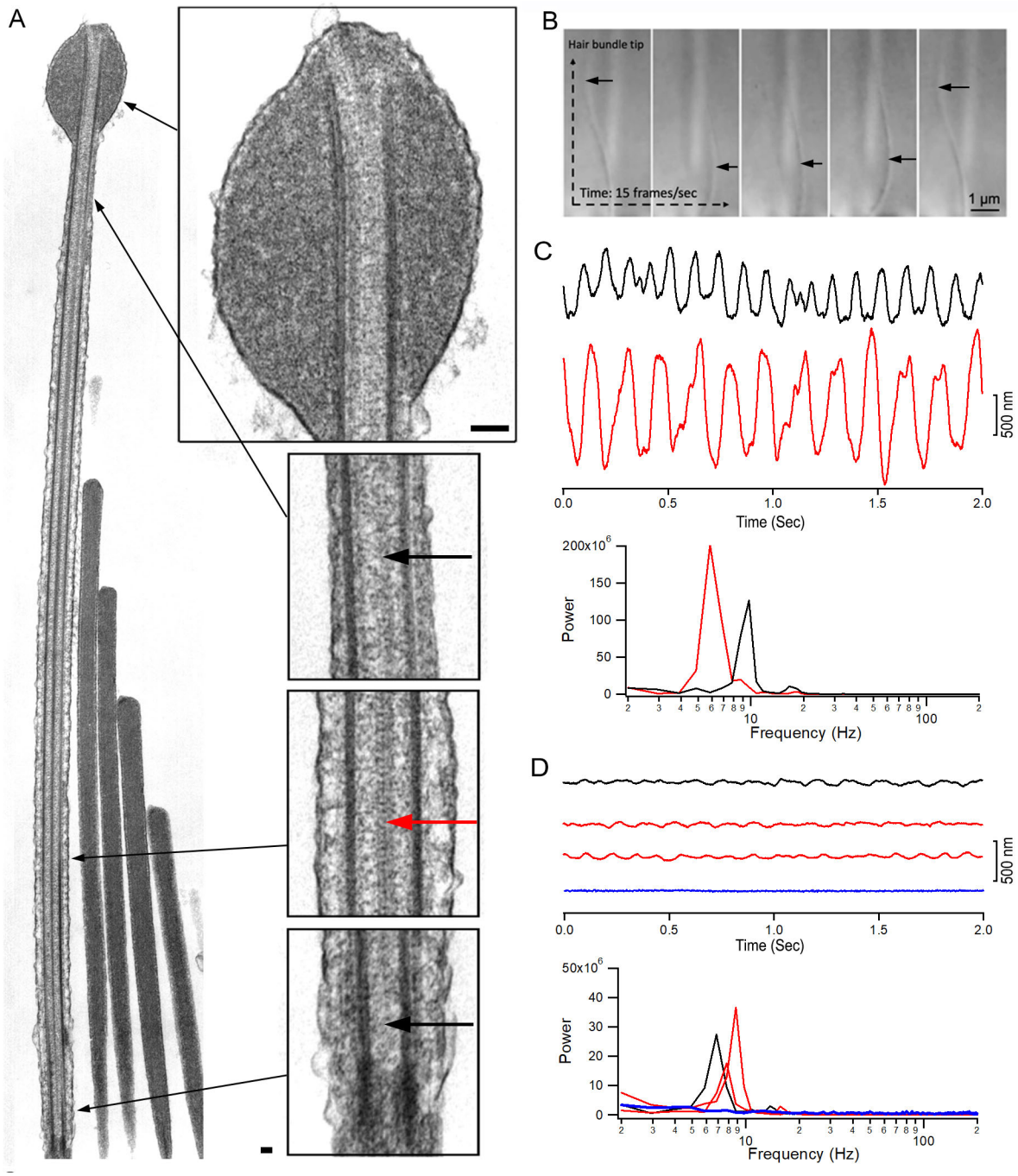
A
B
Hair bundle tip
Time: 15 frames/sec
1 µm
C
500 nm
0.0
0.5
1.0
1.5
2.0
Time (Sec)
200x10^6
150
100
50
0
Power
10
100
Frequency (Hz)
D
500 nm
0.0
0.5
1.0
1.5
2.0
Time (Sec)
50x10^6
40
30
20
10
0
Power
10
100
Frequency (Hz)

Figure 7

A

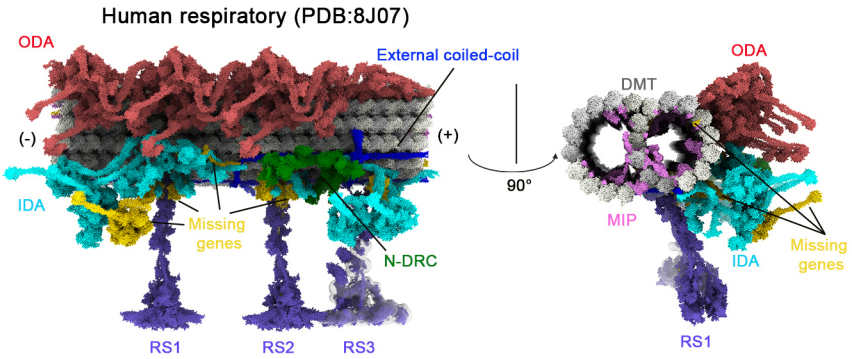

B

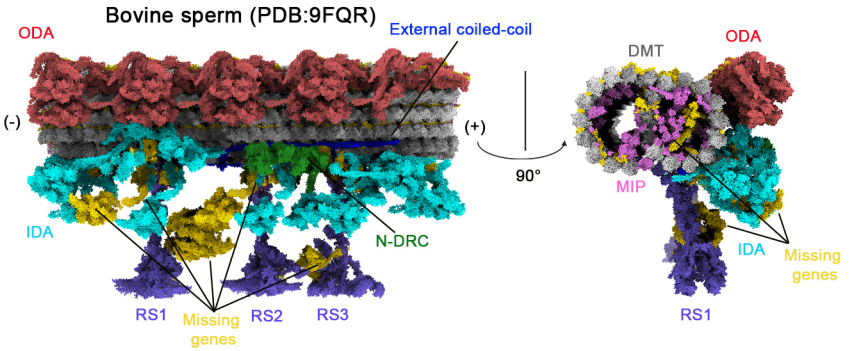

C

Compartment	Missing genes	Effect on motility	Cilia-related disease	Sperm specific
IDA	CCDC37	Unknown	Unknown	No
IDA	DNAH3	Reduced sperm motility (mouse and human)	Male infertility, MAAF (mouse and human)	No
IDA	DNAH12	Sperm immotility	Male infertility, MAAF (mouse and human)	No
IDA	ACTA2	Unknown	Unknown	No
IDA	TEX47	Unknown	Unknown	Yes
RS	MORN3	Unknown	Unknown	No
RS	CAMK4	Reduced sperm motility (human)	Male infertility	Yes
RS	EFCAB5	Unknown	Abnormal testis morphology	Yes
RS	LRRD1	Unknown	Unknown	Yes
RS	STKLD1	Unknown	Unknown	Yes
RS1/2	TRiC	Unknown	Unknown	Yes
ODA	CCDC63	Sperm immotility	Male infertility (mouse)	Yes
MAP	WDR64	Unknown	Unknown	Yes

Figure 8